INVESTIGATING THE USE OF PRECISION CELLULAR BIOPATTERNING FOR GENERATING FUNCTIONAL SKIN EQUIVALENTS

by

Rishima Agarwal

Submitted in partial fulfilment of the requirements
for the degree of Master of Applied Science

at

Dalhousie University
Halifax, Nova Scotia
April 2018

TABLE OF CONTENTS

LIST OF TABLES ..... **v**

LIST OF FIGURES ..... **vi**

ABSTRACT ..... **viii**

LIST OF ABBREVIATIONS USED ..... **ix**

ACKNOWLEDGEMENTS ..... **xi**

CHAPTER 1: INTRODUCTION **1**

1.1. Structure and Function of Skin 1

1.1.1. Epidermis 1

1.1.2. Basement Membrane 3

1.1.3. Dermis and Hypodermis 4

1.2. Skin Injuries and Wound Classification 5

1.2.1. Definition and Classification of Wounds 5

1.2.2. Classification of Skin Injuries 6

1.3. Wound Healing 7

1.3.1. Hemostasis 7

1.3.2. Inflammation 8

1.3.3. Proliferation 8

1.3.4. Maturation 11

1.4. Management of Large and Chronic Wounds 12

1.4.1. Skin Substitutes 13

1.4.2. Cell-Based Therapies 16

1.5. Summary of Current Skin Substitutes 17

1.6. Epithelial Biopatterning Approaches 18
1.6.1. Inkjet-Based Bioprinting (IBP) 19
1.6.2 Laser-Assisted Bioprinting (LaBP) 20
1.6.3. Extrusion-Based Bioprinting (EBP) 21
1.7. Aqueous Two-Phase Systems (ATPSs) 22
1.8. Thesis Aims 26
1.8.1. Aim 1 27
1.8.2. Aim 2 27
1.8.3. Aim 3 28
CHAPTER 2: MATERIALS AND METHODS 29
2.1. Cell Line 30
2.2. Preparation of Polymer Systems 30
2.3. Determination of the Phase Separation Diagram 31
2.4. Determination of Optimal Concentrations of ATPSs-based Inks 33
2.5. Cell Culture 33
2.6. Biopatterning of Keratinocytes on Standard Tissue Culture Plates 34
2.7. Cell Viability Assessment 36
2.7.1. Image Analysis 36
2.8. Cell Proliferation and Formation of Adherens Junctions 37
2.8.1. Cell Proliferation Analysis 37
2.8.2. Formation of Adherens Junctions 38
2.9. Biopatterning of cells on Acellular Dermal Matrices 39
2.10. Cell Engraftment Assessment 40

2.11. Histology and Immunohistochemistry 40
2.12. Statistical Analysis 42
CHAPTER 3: RESULTS & DISCUSSION 43
3.1. Characterization of ATPS-based Inks for Cell Delivery 43
3.1.1. Rationale 43
3.1.2. Optimization of Polymer Concentrations for ATPS EBP of HEK001 Cells 44
3.1.3. ATPSs as a Potential Ink for EBP 50
3.2. Biopatterning of Keratinocytes on Tissue Culture Plates 54
3.2.1. Rationale 54
3.2.2. Cell Viability Assessment 56
3.2.3. Assessment of Cell Proliferation and Formation of Adherens Junctions 60
3.3. Biopatterning of Keratinocytes on DermGEN™ 69
3.3.1. Rationale 69
3.3.2. Biopatterning of Keratinocytes on DermGEN™ 71
3.3.2. Cell Engraftment Analysis 74
3.3.3. Cell Proliferation and Formation of Adherens Junctions on DermGEN™ 76
CHAPTER 4: CONCLUSION 82
4.1. Statement of Contributions 84
4.2. Future Work 85
BIBLIOGRAPHY 87
APPENDIX A: Cambridge University Press Copyright License 96

LIST OF TABLES

Table 1 Assessment of ATPS Formulations for Cell Patterning..... 47

LIST OF FIGURES

Figure 1 An example of a phase separation diagram of PEG 35 kDa - DEX 500 kDA (adapted from Agarwal et al., 2017) 24

Figure 2 Cartoon representation of the cell delivery approaches. 28

Figure 3 Specific methods used for each aim of the study. 29

Figure 4 Cartoon representation of the ATPS EBP cell patterning protocol. 35

Figure 5 Phase separation diagram of PEG 35 kDa and DEX 500 kDa determined using the turbidimetric titration method. 45

Figure 6 Representative images (2X) of equilibrated and non-equilibrated ATPS formulations for cell delivery. 49

Figure 7 Representation images (2X) of cells patterned in ATPS, PEG-alone, DEX-alone, and CM. 52

Figure 8 Cell viability assay. 58

Figure 9 Quantification of calcein-AM and propidium iodide expression in HEK001 cells. 60

Figure 10 Representative images (2X) of the patterned colonies over time. 61

Figure 11 Cell proliferation assay. 63

Figure 12 Quantification of Ki-67 expression in HEK001 cells. 64

Figure 13 Formation of adherens junctions. 66

Figure 14 Quantification of relative expression of E-cadherin junctions in HEK001 cells. 67

Figure 15 Biopatterning of cells on DermGEN™. 72

Figure 16 Representative images (10X) of Hoechst-labelled cells growing on DermGEN™. 73

Figure 17 Cell engraftment on DermGEN™ using patterned and dispersedly-seeded cell delivery approaches. 75

Figure 18 Representative images (20X) of Hematoxylin (purple) and Eosin (pink) (H&E) comparing cell engraftment and stratum basale formation in both patterned and dispersedly-seeded conditions. 78

Figure 19 Representative images (10X) of Ki-67 (red) comparing stratum basale formation in both patterned and dispersedly-seeded conditions. 79

Figure 20 Representative images (10X) of E-cadherin (green) and Hoechst (blue) comparing stratum basale formation in both patterned and dispersedly-seeded conditions. 80

ABSTRACT

The production of skin equivalents for treating full-thickness wounds has been a long-standing challenge in the field of skin tissue engineering. Although several techniques (e.g., skin substitutes and cell-based therapies) have shown promise in restoring extensive skin loss, these approaches are cost-prohibitive and require a large number of autologous cells to accelerate wound healing. As a result, precision biopatterning approaches have been used to improve epidermal regeneration. One of the most commonly used biopatterning approaches for printing cells is extrusion-based bioprinting (EBP). While efficient, the standard bioinks can result in loss of pattern fidelity on moist and irregular, complex substrates. This limitation can be overcome using aqueous two-phase systems (ATPSs). ATPSs involve two or more phase-separating polymers, such as PEG and DEX, that can pattern cells precisely and retain pattern fidelity. Using this approach, ATPS EBP was applied as a novel cell delivery method to promote growth and differentiation of human epidermal keratinocytes cells (HEK001) on both standard tissue culture plates and acellular dermal matrices (DermGEN™). In order to demonstrate the application of ATPS EBP, optimal concentrations of PEG and DEX were identified for stable pattern formation and cell viability. The results from these experiments suggested that 5.0% PEG and 5.0% DEX resulted in a stable interface and pattern formation on wet substrates. This formulation was selected for precise patterning of cells. Using 5.0% PEG and 5.0% DEX, cells were patterned in colonies to promote cell expansion and differentiation in culture. As a control, the same number of cells were dispersedly-seeded on standard tissue culture plates. The efficiency of the ATPS EBP method was evaluated by comparing the differences in growth properties of keratinocytes between the patterned and dispersedly-seeded conditions. Cells patterned in colonies on tissue culture plates displayed superior cell viability as well as improved barrier formation than cells in the dispersedly-seeded condition. Finally, the clinical application of ATPS EBP was demonstrated by patterning the cells directly on DermGEN™ (an acellular dermal matrix that retains the properties of native dermal tissue) as a model for patterning cells directly on tissues. Cells patterned in discrete colonies on acellular dermal matrices were able to preserve their pattern fidelity, suggesting that ATPS EBP can be used to print biomolecules on complex, non-uniform substrates. Moreover, cells patterned in colonies on DermGEN™ demonstrated improved cellular engraftment and stratum basale formation compared to cells in the dispersedly-seeded condition. These findings suggest that biopatterned cells using ATPS EBP holds promise in promoting epidermal regeneration, which may be useful for generating functional skin equivalents.

LIST OF ABBREVIATIONS USED

3D	Three-dimensional
% wt	Percent weight
°C	Degrees Celsius
ADE	Acoustic droplet ejection
ADP	Adenosine diphosphate
AM	Acetoxymethyl
ANOVA	Analysis of variance
ATPS	Aqueous two-phase systems
AU	Arbitrary units
bFGF	Basic fibroblast growth factor
Blue-Dex	Blue-dextran
BSA	Bovine serum albumin
Ca^{2+}	Calcium ion
C-AM	Calcein-AM
CEA	Cultured epidermal autograft
C_f	Final concentration
C_i	Initial concentration
CM	Culture medium
CO_2	Carbon dioxide
DEX	Dextran
dH_2O	Distilled water
DMEM	Dulbecco's modified eagle's medium
DNA	Deoxyribonucleic acid
EBP	Extrusion-based bioprinting
ECM	Extracellular matrix
EGF	Epidermal growth factor
EGFR	Epidermal growth factor receptor
FBS	Fetal bovine serum
FGF	Fibroblast growth factor
H&E	Hematoxylin and Eosin
HEK001	Human epidermal keratinocytes
IBP	Inkjet-based bioprinting
IgG	Immunoglobulin
IL-1	Interleukin-1
kda	Kilodalton
K-SFM	Keratinocyte-serum free medium
LaBP	Laser-assisted bioprinting
MESCs	Mouse embryonic stem cells
mins	Minutes
mL	Milliliter
mM	Millimolar
NBF	Neutral buffered formalin
ng	Nanogram

PAF	Platelet-activating factor
PBS	Phosphate buffered saline
PBST	Phosphate buffered saline with Tween 20
PCL	Polycaprolactone
PDGF	Platelet-derived growth factor
PEG	Poly(ethylene glycol)
PI	Propidium iodide
PLGA	Poly(lactic-co-glycolic) acid
rcf	Relative centrifugal force
RLU	Relative light units
ROIs	Regions of interest
SC	Stratum corneum
SD	Standard deviation
T	Temperature
t	Time
T500	Technical grade DEX 500kda
TGase	Transglutaminase
TGF-ß	Transforming growth factor- ß
TNF-α	Tumor necrosis factor- α
TXA2	Thromboxane A2
UV	Ultraviolet
VEGF	Vascular endothelial growth factor
V_f	Final volume
V_i	Initial volume
γ_{12}	Interfacial energy
ΔG	Change in Gibbs free energy
ΔH	Change in enthalpy
ΔS	Change in entropy
θ	Contact angle
µL	Microliter
µm	Micrometer

ACKNOWLEDGEMENTS

I would like to extend my sincere thanks to everyone who has supported me throughout my Master's program. In particular, I want to thank my supervisor, Dr. John Frampton, for his excellent mentorship and guidance over the course of my degree. Thank you for taking me under your wing, showing me the ropes, and for providing me with numerous opportunities and for all your unwavering support over the years. I can't thank you enough for providing me with the opportunity to work within an industry. It has been a fantastic learning experience. You taught me the true meaning of research and have helped me develop as a researcher. Your passion for research and optimism is something that has inspired all of us. Thank you for your patience, continual brainstorming and encouragement to think outside the box. You are a perfect example of what a supervisor should be and I am very grateful to be a part of the Frampton Lab.

I would also like to extend my sincere thanks to my committee members for providing me with insightful feedback and expertise throughout the course of my thesis project:
Dr. Brendan Leung, Dr. Robert Adamson, and Dr. Paul F. Gratzer. I have learned a lot under your mentorship. Additionally, I would kindly thank Dr. Gratzer and DeCell Technologies for providing the DermGEN™ samples for this study. Without your generous support, this work would not have been possible.

I would like to give thanks to my lab members for providing me with support and encouragement throughout the years: Angela Tsai, Leo Liu, Nicky Tam, Beatrice Chang, Mackenzie Ruthven, Hady Sarhan, Connor Lamont, and Maia Kvas. It has been a privilege

to work with wonderful people like you and thanks for making the lab to be a more enjoyable place to work at. A special thanks to Leo Liu and Nicky Tam for all their help with the cell viability data analysis. To Alyne Teixeira, thank you for being the best roommate and an amazing friend! It has not been easy for us, but having you by my side made this journey a lot easier. Thank you for always being there for me and for inspiring me in so many ways. All the late-night chats that we had in your room will be missed.

This journey would not have been possible without the love and support of the two most important people in my life: Kristin Robin Ko and Sarah McLeod. Kristin and Sarah, I don't think any words can describe the level of gratitude and love that I have for you two. You two have been my biggest support system over the past few years, so thank you for being my rock and anchor, and for keeping me grounded when I thought I would blow away. You two have always encouraged and inspired me to become a better person. You both have always stood by me through thick and thin and through sickness and in health. You have heard all my complaints, taken my mood swings, fed me, took me to the hospital at midnight, supported me in my most difficult times (the list goes on) and did everything that a family would do. I will cherish our friendship for a lifetime. Thank you for being the shoulder that I could always depend on. I can't wait for our trip to Barcelona. For fame and glory!

I would like to thank my family members who mean the world to me. To my mom and dad, Shalini Goel and Rajeev Goel, I am truly grateful to you and for all the unconditional love and support you have provided me throughout my life. Mom and Dad, thank you for

teaching me the value of knowledge and hard work, for always believing in me, and for giving me freedom to choose what I desired. Thank you to my brother and sister-in-law, Mrigank Agarwal and Akshita Bansal, for continuing moral support, love and understanding. I have complained a lot over the past few years, but your words of encouragements have always helped me achieve my goals. Mrigank, thank you for being my role model and second mom, a mentor, friend, and an incredible brother. I wouldn't be where I am today without all of you.

Finally, I would like to acknowledge all the funding agencies and grants that have supported this work: the Canadian Institutes of Health Research (CIHR), the Dalhousie University Faculty of Engineering (Exxon Mobil Canada Ltd.), Canada Research Chairs Program, Canada Foundation for Innovation (Project# 33533), and the Natural Sciences and Engineering Research Council of Canada (NSERC - RGPIN-2016-02498)

CHAPTER 1: INTRODUCTION

1.1. Structure and Function of Skin

Skin is the largest organ of the body that accounts for approximately one-tenth of the body mass. It is the first line of defense that provides an effective barrier against the entry of toxins and microorganisms, and retains fluid in the body to prevent dehydration. Skin also plays a crucial role in other important functions including immune surveillance, sensation, and maintenance of homeostasis (*1–4*). Skin is primarily comprised of three layers: the epidermis, dermis, and hypodermis.

1.1.1. Epidermis

The epidermis is the outermost layer of the skin that is separated from the dermis by a basement membrane. The epidermis is avascular, so it is nourished by diffusion from blood vessels of the underlying dermis (*4–6*). It is primarily composed of keratinocytes that impart structural strength and resilience. In addition to keratinocytes, there are other cell types that are present in the epidermis, including Merkel cells, melanocytes, and Langerhans' cells (*4–8*). Merkel cells are specialized mechanoreceptors that responds to light touch. These cells are distributed throughout the basal layer of the epidermis, and can detect a skin displacement of less than 1mm (*4–6*). Melanocytes reside in the basal layer of the epidermis, where they contribute to the skin colour and protect the skin from the harmful effects of ultraviolet (UV) light (*4*). Finally, the Langerhans' cells are antigen

presenting cells that play an important role in the immune system (*4*, *5*).

Structure of the Epidermis

The epidermis is a squamous epithelium composed of five strata: stratum basale, stratum spinosum, stratum granulosum, stratum lucidum, and stratum corneum (SC). The stratum basale is anchored to the basement membrane by hemidesmosomes, while the keratinocytes are held together by desmosomes. Both hemidesmosomes and desmosomes are responsible for providing structural strength to the stratum basale. The stratum basale harbours highly proliferative cells and self-renewing populations of keratinocytes. The epidermis undergoes continual proliferation for renewal of the outer layer of epidermis. As keratinocytes undergo mitosis in the stratum basale, the cells get pushed towards the surface of the epidermis where they mature and differentiate. These terminally differentiated cells are important for the development of the stratum corneum, the uppermost layer of the epidermis (*5*, *7–9*). The process of epidermal stratification is further discussed below.

Stratification of the epidermis

Stratification of the epidermis can be defined as the formation of several layers of differentiated cells. As the cells in the epidermis undergo mitosis, one daughter cell becomes a new stratum basale cell that can divide again, whereas the other daughter cell gets pushed outward towards the surface. As cells move from the basal to the spinous layer, they initiate the process of terminal differentiation. As the cells move to the spinous layer, the expression of genes encoding keratin 5 and keratin 14 (intermediate filament proteins

that are expressed only in the stratum basale layer) subsides and the genes encoding keratin 1 and keratin 10 begin to express. These intermediate filament proteins are interlinked with the desmosomes to form a robust cytoskeleton network that provides resistance against mechanical stresses (*4*, *10–14*). Moreover, the lamellar bodies (membrane bound-organelles containing lipids, keratin fibers, and hydrolytic enzymes) start to appear in the keratinocytes. The lamellar bodies are eventually secreted from keratinocytes to form an impermeable, lipid membrane, which protects the skin against water loss (*4*, *10–15*).

During the later stages of terminal differentiation, the cells withdraw from the cell cycle. The epidermal differentiation process generates proteins such as involucrin and loricrin, which are cross-linked by transglutaminase (TGase) 1 to form a "cornified envelope". Moreover, keratohyalin granules begin to accumulate in the cytoplasm of the cells. The keratohyalin granules are comprised of keratin filaments and profilaggrin. Profilaggrin dephosphorylation causes keratin filaments to aggregate. Simultaneously, the nucleus and other organelles in the cells disintegrate, resulting in dead cells with a cornified envelope that is mainly composed of keratins. Finally, the lamellar bodies release their lipid contents around the dead cells to form the outermost layer of the epidermis, i.e, the stratum corneum (SC). The keratins and the cornified envelope contribute to mechanical resistance of the SC, while the waxy lipid substance around the cells serves as a water barrier (*4*, *10–18*).

1.1.2. Basement Membrane

The epidermis and the underlying layer of dermis are separated by a porous basement membrane. The basement membrane is approximately 50 - 70 nm thick and contains two

layers: lamina lucida and lamina densa. The lamina densa is primarily composed of type IV collagen and perlecans. On the other hand, the lamina lucida consists of laminin and nidogen. The main function of the basement membrane is to provide structural support to the epithelium. It also allows the exchange of nutrients and waste between the two layers (*4*, *19–21*).

1.1.3. Dermis and Hypodermis

The dermis is the middle layer of skin, which contains extracellular matrix (ECM) proteins, fibroblasts, immune cells, and a variety of other cells that help to impart tensile strength and flexibility. The strength and toughness of dermis is maintained by collagen fibers, while elastin provides elasticity and flexibility (*1–8*). The dermis also houses the skin appendages (e.g., sweat glands and hair follicles), nerve endings, and sensory neurons that play a crucial role in regulation of temperature, pain and pressure, respectively (*22*). The dermis consists of two layers, the papillary and reticular layers. The papillary layer has loosely arranged collagen fibers and a large number of blood vessels that provide nutrients to the epidermis through the basement membrane. The reticular layer is continuous with the hypodermis. It has a variety of dense and irregular fibers that are resistant to stretching (*1–8*).

Finally, the hypodermis or subcutaneous tissue is the deepest layer of skin that separates the dermis from the underlying muscle and bone. This layer is mainly composed of adipocytes and loose connective tissue made up of collagen and elastin fibers. It also consists of other cell types including fibroblasts and macrophages. The hypodermis is

responsible for providing insulation and serves as a reservoir for energy storage (*4*, *5*, *7*, *8*, *23*).

1.2. Skin Injuries and Wound Classification

As previously mentioned, skin plays an important role in maintaining homeostasis and providing an effective barrier against the outside world. Due to various functions of skin, any damage to the epidermis and dermis can lead to physiological imbalance, causing disability or ultimately death in some cases (*1*). There are several factors that can result in loss of fluid, infections, and scarring. Both the epidermis and dermis can be damaged by genetic conditions (e.g., epidermolysis bullosa), complications from surgery, thermal injuries (e.g., burns), acute trauma, and chronic ulceration (*1*, *24*). Approximately 300 million people worldwide are affected by chronic wounds. This number will escalate due to increasing prevalence of diabetes and peripheral vascular disease (*25*). The most common cause of chronic wounds is thermal injuries i.e., burns. Patients with extensive burns suffer from psychological, physical, and economical burdens. For instance, in Canada, in 2010 the cost related to burn injuries was projected at $366 million. Furthermore, the average healthcare costs per burn patient was estimated at $88,218 as of 2012. Therefore, there is an increasing demand for effective treatments and therapies that can restore skin loss by promoting wound healing.

1.2.1. Definition and Classification of Wounds

Since skin injuries are prominent in both young and elderly populations, researchers and clinicians have been seeking treatments for repairing large wounds. Wounds can be defined

as “damage or disruption to the normal anatomical structure and function” (*26*). This can range from a simple cut in the epidermis to a deeper cut in the skin that can extend to other structures (e.g., muscles and tendons). Wounds can be classified into two categories: acute and chronic wounds. Acute wounds can restore the structure and function of the tissue with minimal scarring within 10-30 days. The primary causes of acute wounds are abrasions and cuts due to external factors and surgical procedures. Acute wounds can also include burns and chemical injuries that are caused by electricity, radiation, and chemicals. On the other hand, chronic wounds fail to progress through the stages of wound healing, and are characterized by slow and incomplete healing of the tissue. Various factors such as persistent infection, large wound surface area, hypoxia, and excessive secretion of inflammatory cytokines can contribute to poor healing outcomes. Diabetes, ulceration, burns, and vasculitis can result in chronic wounds, which can have a significant impact on the quality of life of patients and on the healthcare system (*26*, *27*).

1.2.2. Classification of Skin Injuries

Skin injuries are classified into four categories: epidermal, superficial partial-thickness injuries, deep partial-thickness injuries, and full-thickness injuries. Epidermal injuries include grazing, which can be regenerated rapidly, while superficial partial-thickness injuries include the loss of the epidermis and the superficial part of the dermis. Such wounds heal by re-epithelialization (discussed in section 1.3.3.). Both epidermal and superficial partial-thickness injuries heal normally by progressing through the various stages of wound healing. Deep partial-thickness injuries involve loss of a greater portion of the dermal layer. These injuries heal very slowly and result in evident scar tissues.

Finally, full-thickness injuries are characterized by loss of the epidermis and dermis. Such wounds cannot re-epithelialize on their own and can only heal by contraction (*28*). Therefore, any large injuries greater than 4 cm or more in diameter need grafts or other interventions to restore and repair the damaged tissue (*29*, *30*).

1.3. Wound Healing

Epidermal and superficial partial-thickness injuries repair themselves by the process of re-epithelialization, while deep partial-thickness injuries heal by progressing through the stages of wound healing including granulation tissue formation, contraction, and re-epithelialization. Wound healing is a dynamic inherent response that restores tissue integrity. It involves complex interactions among soluble mediators, cells, and the ECM to restore the integrity of the damaged tissues. Wound healing can be divided into four stages: hemostasis, inflammation, proliferation, and maturation (*31–33*).

1.3.1. Hemostasis

When an injury occurs, hemostasis is the first physiological response that occurs at the wound site. It initiates a cascade of events that include vascular constriction, platelet degranulation, and formation of a fibrin clot (*31*, *34*, *35*). When an injury occurs, the exposed collagen interacts with circulating platelets, which activates the platelets. Activated platelets adhere tightly to each other and to the ECM to form a platelet plug at the site of injury. The platelets degranulate and release their alpha granules (e.g., ADP, platelet-activating factor (PAF), and thromboxane A_2 (TXA_2)) into the blood plasma, which increases secretion and activation of chemokines such as platelet-derived growth

factor (PDGF), interleukin (IL)-1, and transforming growth factor (TGF)-ß. Since these chemokines are continuously released into the blood plasma, more platelets get activated to form the platelet plug at the injury site. Once the platelet plug has been formed, clotting factors are activated to form a fibrin mesh. Some of the white and red blood cells get trapped within the fibrin mesh, and form a clot (*27*, *36*).

1.3.2. Inflammation

Immediately after the clot is formed, neutrophils are recruited to the wound site by various cytokines, including (IL)-1, tumor necrosis factor (TNF)-α, and TGF-ß. Furthermore, prostaglandins are produced by the COX-2 enzyme in the platelets, which vasodilate the blood vessels to facilitate the movement of neutrophils and monocytes to the injured sites. Neutrophils are recruited to the wound within 24-36 hours of injury. Neutrophils release proteolytic enzymes and phagocytose any foreign materials and bacteria. Within 48-72 hours of injury, monocytes enter the wound site. These cells undergo phenotypic changes and transform into macrophages. Macrophages secrete IL-1 and TNF-α, and TGF-ß to stimulate fibroblasts and keratinocytes, respectively. The depletion of macrophages in wound healing can lead to delayed fibroblast and keratinocyte maturation along with delayed angiogenesis, resulting in defective wound repair (*27*, *31*, *37*, *38*).

1.3.3. Proliferation

The proliferative phase starts on the second or third day of the injury and lasts for about two to three weeks. This stage of wound healing is characterized by angiogenesis, epithelialization, and granulation tissue formation.

Angiogenesis

Formation of blood vessels also plays a crucial role in the wound healing process. Many angiogenic factors (e.g., vascular endothelial growth factor (VEGF), platelet-derived growth factor (PDGF) and basic fibroblast growth factor (bFGF)) are secreted to promote the formation of blood vessels. These growth factors bind to receptors on the endothelial cells of existing vessels, which activates a cascade of signaling events. The activated endothelial cells secrete proteolytic enzymes to degrade the existing vascular basal lamina. After the breakdown of the basement membrane, the existing endothelial cells are able to proliferate and migrate towards the wound. Consequently, new blood vessels are formed. This process is called sprouting. These sprouting blood vessels are directed toward the ECM by an endothelial tip cell (a non-proliferating cell at the tip of the capillary sprout that directs migration). Meanwhile, the endothelial cells are still undergoing proliferation to elongate the newly built sprout, which will eventually form a capillary. The endothelial cells also release matrix metalloproteinases to degrade or lyse any surrounding tissue that may interfere with the blood vessel formation. Finally, two or more endothelial tip cells will fuse to form a continuous lumen through which oxygenated blood can flow. The newly built vessel will further differentiate into arteries and venules. Moreover, these vessels will be further stabilized by recruitment of pericytes and smooth muscle cells (*27*, *39*).

Epidermal Restoration

If the basement membrane remains intact after the injury, keratinocytes proliferate and stratify in their normal pattern. However, in cases of wounds with the loss of basement membrane, the restoration of epithelial barrier is accomplished by re-epithelialization, a

process where epidermal cells spread across the wounds. Failure to re-epithelialize a wound results in loss of intact epidermal barrier, and thus, re-epithelialization is a critical and defining feature of wound healing (*40*, *41*). Wound re-epithelialization is dependent on the proliferation capacity and migration of epidermal keratinocytes to cover the denuded surface (*40–42*). Upon injury, keratinocytes (which are usually non-motile) undergo phenotypic alterations in cytoskeleton networks and cell surface receptors that disassemble the keratinocytes from the wound margin and produce a migratory phenotype. This allows keratinocytes to migrate and proliferate over the wound surface until the cells come in contact with each other, resulting in restoration of the skin barrier (*40–44*). However, re-epithelialization becomes challenging in large wounds (even those treated with dermal replacement materials) where cells located at the wound edges lack the ability to re-epithelialize the surface (*43*).

Granulation Tissue Formation

Granulation tissue formation is the final phase of the proliferative stage. Deep partial-thickness injuries are usually restored by granulation tissue formation and wound contraction. During this process, fibroblasts migrate into the wound site where the cells become activated and synthesize collagen. PDGF, epidermal growth factor (EGF), and FGF stimulate fibroblast proliferation. PDGF produced from wound fibroblasts (fibroblasts at the wound site) acts via autocrine and paracrine signaling and further amplifies the proliferation of fibroblasts. Within the wound site, the fibroblasts proliferate significantly and synthesize provisional matrix components including hyaluronan, fibronectin, proteoglycans, and collagen III, which further promote cell migration. Around 7-10 days

after wounding, the fibroblasts transform into myofibroblasts. Myofibroblasts express α-actin, which allows the cells to generate strong contractile forces to pull the edges of the wound together. Finally, once the wound has stopped contracting, the unneeded fibroblasts and myofibroblasts undergo apoptosis (programmed cell death) (*27*, *31*, *37*, *38*).

1.3.4. Maturation

The maturation and remodeling stage begins two to three weeks after the onset of injury and can last up to a year or more. If the collagen deposition is too low, the strength of the remodeled skin will be greatly reduced. However, if excessive collagen is deposited, hypertrophic scar or keloid can result. During this stage, granulation tissue transitions from a disorganized network of collagen III, glycosaminoglycans, and fibronectin to a more organized network of ECM proteins. Matrix metalloproteinases secreted by fibroblasts, endothelial cells, neutrophils and macrophages degrade collagen III, thereby promoting the synthesis of collagen I. The initial collagen fibers deposited on the wound site are thin, but eventually get replaced by thicker fibers, enhancing the tensile strength of the tissue. Further remodeling of the tissue causes a decrease in number of cells via apoptosis, blood flow, and metabolic activity, resulting in a mature scar tissue with a high tensile strength. However, the scar tissue will never have the tensile properties of the uninjured skin (*27*, *31*, *32*, *37*, *38*).

1.4. Management of Large and Chronic Wounds

As mentioned earlier, skin injuries can be divided into four categories: epidermal, superficial partial-thickness, deep partial-thickness, and fill-thickness. In epidermal and superficial partial-thickness injuries, the skin heals through the natural repair response, as described in section 1.3. However, in cases of deep partial-thickness or full-thickness injuries, the normal repair response goes awry, which results in excessive scar tissue formation and chronic wounds. Wounds that are greater than 4 cm or more cannot repair on their own and need a graft to help restore the damaged/diseased skin tissues (*29*, *30*).

The current gold standard for repairing large and chronic wounds is skin autografting (*28*, *45*). In skin autografts, the surgeon uses a specialized surgical instrument called a dermatome to shave a thin layer of skin from the donor site of the patient. The thin skin is then applied to the wound site to help treat skin injuries. Depending on the type of skin injury, skin grafts can be classified in two categories: split-thickness and full-thickness grafts. A split-thickness graft is composed of the epidermis and a portion of the dermis. These grafts can be further divided into thin, intermediate, and thick grafts, and thickness of these grafts ranges from 0.15-0.3 mm, 0.3-0.45 mm and 0.45-0.6 mm, respectively (*45*, *46*). In full-thickness grafts, the entire epidermis and dermis are transplanted to the wound site. These grafts are usually thicker than 0.6 mm (*46*). Autografts have been used to treat some serious skin injuries; however, they may not be the ideal treatment for patients with severe wounds due to limited availability of donor sites. These procedures also create wounds at donor sites that may result in scar formation and/or other severe complications.

Therefore, there is a strong demand for an alternative treatment that is able to restore both the epidermis and dermis in patients with extensive skin loss.

Tissue engineering has shown significant promise in improving the wound healing process. Tissue engineering aims to fabricate tissues and organs by using a scaffolding material to provide a supportive matrix for appropriate tissue growth and repair. The goal of many current skin tissue engineering approaches is to create a functional equivalent skin substitute that can restore the epidermal barrier. Although there are no ideal skin substitutes, these engineered constructs should: **(1)** prevent water loss and form an epidermal barrier, **(2)** be cost-efficient, **(3)** have a long shelf life and be easy-to-use, **(4)** participate in a positive host immune response, **(5)** work on irregular wound surfaces, **(6)** require one surgical procedure, **(7)** have long-term durability and **(8)** provide permanent wound coverage. Although we are far from creating a skin substitute that possesses these ideal characteristics, several attempts have been made to create tissue-engineered products that may aid in restoring damaged and/or diseased skin. These products are classified into two categories: skin substitutes and cell-based therapies, which are further discussed below (*24*).

1.4.1. Skin Substitutes

Over the years, progress in tissue engineering has led to development of several types of skin substitutes that facilitate wound healing. The history of skin tissue engineering can be traced back to the 1970s when the cultured epidermal autograft (CEA) was developed as a treatment for burn victims (*47*). O'Connor and colleagues were the first group to

demonstrate the use of CEA as a skin substitute. In their study, epidermal cells taken from a $2cm^2$ biopsy were cultured for three weeks and were able to successfully restore skin loss in adult patients. This breakthrough finding was important for the development of many commercialized skin substitute products.

One such example is Epicel®: a sheet composed of 2-8 layers of autologous keratinocytes attached to a petrolatum gauze. It has been recommended for patients that have damage to ≥ 30% of total body surface area. Epicel® grafts are not at risk of rejection by the recipient's immune system because they use autologous keratinocytes (*48*). Patients who received Epicel® as a potential treatment showed a survival rate of 86.6%; however, some serious events were observed as indicated by a 13% death rate and 14% infection rate (*48*). Despite high survival rates, there are many challenges that prevent the clinical use of CEAs. Firstly, the timing of CEA is an important concern for surgeons. A CEA takes approximately three weeks to produce, so it may not be readily available for patients who need immediate treatment. In some cases, even though the CEA may be ready, the patient may not be ready to undergo surgery, and thus the efficacy of the keratinocyte sheet is reduced and results in poor clinical outcomes. Secondly, the CEA sheets are very fragile and are sensitive to stress, making them inappropriate for use around joints. CEAs also lack the dermal bed and are of limited value without an already well-vascularized dermal bed. Finally, a CEA is very expensive to produce, limiting its use in many clinical settings (*29*, *48*, *49*).

Since CEAs lack a vascularized dermal bed and have poor mechanical stability, they cannot be used to treat full thickness wounds without wound contractions and/or scars. Thus,

attempts have been made to develop other cell-based skin substitutes. For instance, Dermagraft® (a human fibroblast-derived skin substitute) can help restore the dermal bed by allowing epithelial cells to migrate over and close the wound (*50*, *51*). Dermagraft® is composed of fibroblasts, ECM, and a bioabsorbable polyglactin mesh scaffold in which fibroblasts are cultivated. The cells proliferate and secrete collagen, ECM proteins, and growth factors to produce a dermal matrix (*50*, *51*). Gentzkow et al. evaluated the effectiveness of Dermagraft® in 50 patients with diabetic foot ulcers over a 12-week period (*52*). Patients treated with Dermagraft® (50% healed ulcers) had better healing than the control group (8% healed ulcers). Moreover, this study demonstrated that the patients who received Dermagraft® every week healed significantly better than the patients who received it bi-weekly or monthly. Other studies have also indicated that Dermagraft® is effective for treating wounds like diabetic foot ulcers (*50*, *51*). However, this product failed clinical trials for venous ulcers as Dermagraft® was unable to completely heal the wound by 16 weeks. Moreover, the product has a prohibitive cost along with inconsistent clinical outcomes, which makes it unappealing for future use (*53*–*55*).

Acellular human dermis (e.g., GraftJacket®) has also been investigated for skin reconstruction. Graftjacket® is derived from donated human skin that has been processed to remove any immunogenic components while persevering a matrix that retains the biochemical and structural components of ECM important for revascularization, recellularization and reintegration (*56*). Despite its moderate clinical success, low healing rates and inconsistent performance have been observed, which is attributed to the failure to remove donor cellular components (*57*, *58*). DeCell Technologies Inc. have recently

developed a decellularized tissue scaffold called DermGEN™ derived from human donated skin in order to address the unmet need for effective treatment for wounds. DeCell Technologies have developed a proprietary novel decellularization process, which promises to remove cellular components more effectively than the existing decellularization techniques (*59*). The main product from DeCell Technologies (DermGEN^{TM}) will be used in this thesis as an acellular dermal material for engraftment of epidermal cells.

1.4.2. Cell-Based Therapies

Although biomaterials such as acellular scaffolds have shown significant promise in tissue engineering, they lack the ability to fully heal cell-rich tissues surrounding some wounds. Therefore, cell-based therapies have been exploited for wound reconstruction. These cell-based therapies use autologous cells to accelerate the wound healing process (*60*). As a result, researchers have investigated the use of composite skin for permanent wound coverage. Composite skin involves the combination of a dermal skin substitute along with a CEA to improve the wound healing process (*61*). Gallico et al. first reported a case study in which composite skin was used as a strategy for skin replacement. In this study, the patient received a collagen-glycosaminoglycans dermal matrix followed by CEA. The composite skin graft performed well and the patient was able to recover from skin loss (*62*). Although these grafts have shown promising results, composite skin grafts have barely been used for repairing large wounds. One of the main reasons for the limited use of composite grafts is the cost. Both dermal skin substitutes and CEAs are very expensive, which makes this more expensive and difficult to use compared to other commercially

available therapies. Another limitation of using the two step-procedure is the lack of engraftment. Moreover, like CEAs, the composite sheets are fragile and difficult to handle (*63*).

To overcome the difficulties of composite skin, cell seeding and cell spraying approaches have also been examined to deliver cells on a scaffolding material for restoring the damaged and/or diseased skin (*60*, *64*). The most commonly used biomaterials include natural hydrogels (e.g., alginate, gelatin, alginate, and fibrin) and synthetic materials (e.g., polycaprolactone (PCL) and poly(lactic-co-glycolic) acid (PLGA) (*24*). Since these methods rely on manual cell seeding or spraying, they are unable to emulate the complexities of native tissue and therefore are unable to reflect accurate physiological responses. This becomes particularly challenging in fabricating a cell-dense construct such as the epidermis where the tissue formation is based on cell assembly. Although many tissue engineering strategies have been utilized to develop skin substitutes, these techniques are unable to reliably promote cell-cell interactions and cell-matrix interactions.

1.5. Summary of Current Skin Substitutes

The production of skin substitutes has been a long-standing challenge in the field of tissue engineering. Although many strategies have been developed for skin reconstruction, we have not been able to successfully generate a multi-layered structure with skin appendages and other glands. Most of the skin substitutes used for skin reconstruction are predominantly acellular in nature. These acellular dermal components are beneficial for stabilizing the dermal wound bed, but are unable to full support epidermal reconstruction

for chronic wounds. This becomes problematic for large wounds as the cells in the wound margin lack the ability to re-epithelialize, and are unable to restore the structure and function of the skin. The most frequently used approach for epidermal reconstruction is to grow and expand autologous keratinocytes in culture. This process, however, takes weeks to grow and involves long waiting times, which may not be feasible for patients seeking immediate medical treatment. Furthermore, when epidermal sheets are combined with acellular dermal matrices, poor cell engraftment has been observed. As an alternative, cell seeding and cell spraying options have also been considered for skin reconstruction. These methods also rely on autologous cells, but are limited by the availability of cells. Moreover, the low precision delivery of these techniques prevents the cells from being delivered efficiently, and therefore are unable to generate a complex construct that mimics the structure and function of skin. Therefore, it is important for researchers to develop strategies that will allow the cells to expand in culture and promote cell-cell and cell-matrix interactions once placed at a target site.

1.6. Epithelial Biopatterning Approaches

Advances in biopatterning techniques have allowed researchers to investigate the effects of homotypic and heterotypic interactions on cell proliferation, growth, and differentiation. In contrast to cell seeding and cell spraying approaches, biopatterning approaches can be used to precisely deliver cells in a predefined arrangement with the goal of promoting rapid re-epithelization. Biopatterning is often interchangeably used with the term “bioprinting”. In this context, biopatterning allows precise positioning of cells, proteins, growth factors, and/or bioactive molecules to improve and study cell-cell interactions, cell migration, cell

proliferation, and cell differentiation (*65*). Biopatterning was first demonstrated as cytoscribing in 1988 when Klenn used a Hewlett-Packard inkjet printer to position cells at a precise location (*66*). It is one of the emerging techniques that has been utilized in many fields including regenerative medicine, tissue engineering, and pharmaceutical testing. Biopatterning has been used to fabricate a wide variety of tissues including bone, skin, liver, cartilage, and cardiac tissue (*67*). There are several biopatterning approaches that are being used for fabricating tissue and/or organs. Cutting-edge approaches currently under development include inkjet-based bioprinting (IBP), laser-assisted bioprinting (LaBP), and extrusion-based bioprinting (EBP).

1.6.1. Inkjet-Based Bioprinting (IBP)

IBP is a non-contact patterning method that allows the deposition of cell-rich droplets on a substrate (*68*). The working principle of IBP is similar to that of desktop inkjet printers where the print head can be actuated either thermally or piezoelectrically. In thermally actuated IBP, a pressure is generated in the reservoir tank that contains the bioink. The pressure inside the tank forms bubbles that forces the bioink out through the orifice and the cell-rich bioink gets deposited on the substrate. The thermally actuated inkjet printers are not expensive and can print a wide variety of low viscosity biomaterials with high speed (<10,000 droplets/seconds) (*68*–*70*). However, the cells have relatively low cell viability due to exposure to high temperature and mechanical stress. Moreover, the nozzle in IBP results in frequent clogging, which presents a threat to smooth printing. Finally, thermal inkjet printers result in non-uniform drop sizes which restricts their use in three-dimensional (3D) bioprinting (*68*, *69*).

1.6.2 Laser-Assisted Bioprinting (LaBP)

LaBP uses a pulsed laser beam to position cells onto a substrate. The LaBP set-up consists of a laser beam, a donor glass slide coated with a laser-energy-absorbing layer (e.g., gold or titanium) containing a thin layer of biological materials, and a collector substrate. In LaBP, a laser beam is focused on the donor slide to vaporize the metal layer, which results in the production of cell containing droplets that get propelled towards the collector substrate (*71*, *72*). Recently, Michael et al. generated a bilayered skin construct using LaBP. In this study, 20 layers of NIH-3T3 fibroblasts were printed first followed by 20 layers of HaCat keratinocytes on a sheet of Matriderm® (acellular dermal substitute), and were assessed for formation of gap junctions and cell proliferation. Michael and colleagues also demonstrated the use of LaBP by printing fibroblasts and keratinocytes on Matriderm® (acellular dermal substitute) to create a functional 3D skin substitute as a potential treatment for burn victims. The researchers found that the printed keratinocytes were able to initiate differentiation and formed a multilayered epidermis. Moreover, the printed fibroblasts were able to infiltrate the Matriderm® (*73*).

LaBP has shown significant promises in the field of skin tissue engineering. Like other printing techniques, LaBP also offers may advantages. Since LaBP is nozzle-free, it does not have issues with clogging of biological materials and can therefore print the cells with higher density – a major limitation of other biopatterning techniques. Moreover, LaBP is compatible with various viscous biomaterials (*68*). LaBP can print cell densities up to 10^8/ml at a speed of 1600 mm/S. Although LaBP can print cells precisely on a substrate with high resolution, it is expensive and requires specialized training which may not be

feasible for translation in life sciences. Also, LaBP deposits cell-rich droplets by vaporizing the metal film, which may subject the sample to metal particle contamination. Finally, cells encapsulated in thin layers of hydrogel can dehydrate in air, resulting in low cell viability (*68*).

1.6.3. Extrusion-Based Bioprinting (EBP)

EBP overcomes many of the limitations of LaBP and IBP and therefore is the most widely used biopatterning approach. EBP systems have a dispensing mechanism and a stage that is capable of moving in x, y, and z. These systems use either pneumatic or mechanical fluid displacement to extrude a fluid through a nozzle. The pneumatic-based system uses pressurized air to dispense cells on a substrate, while the mechanical fluid displacement system relies on piston or screw to deposit cells. The screw-based mechanical system provides spatial control and can print high-viscosity materials, while the piston-driven mechanical system offers direct control over the material flow (*74*).

As compared to the other bioprinting approaches, EBP systems typically require less complex instrumentation and are compatible with a broad range of viscous bioinks. Due to the versatility and affordability of this technique, extrusion-based printers have been used to print a variety of cells (*75*) and tissue constructs (*76*). For instance, Kim et al. used a pneumatic driven extrusion-based system to print a collagen and alginate scaffold on a cryogenic stage. This scaffold was then co-cultured with keratinocytes and fibroblasts to fabricate a functional dermal skin substitute (*77*). More recently, Lee et al. also used EBP to generate skin-like tissue by printing alternating layers of collagen I, keratinocytes and

fibroblast (*78*). EBP can print at a very high cell density, which is essential for generating complex cell-rich 3D tissues. Despite these benefits, decreased cell viability is observed when cells are printed using EBP. This might be due to the dispensing pressure which generates shear forces that may adversely affect cell viability (*65*, *68*). Another major limitation of EBP is that the printed pattern fidelity is sometimes lost when the bioink is deposited in cell culture medium or on a wet substrate (*79*). Thus, there is a need for novel bioink formulations that allow the cells to retain their viability and can print with high-pattern fidelity on wet substrates required for many skin tissue engineering applications.

1.7. Aqueous Two-Phase Systems (ATPSs)

A potential bioink for use with EBP is aqueous two-phase systems (ATPSs), which allows cells to be printed on substrates immersed in liquid without the loss of pattern fidelity. ATPS-based inks utilize two or more biocompatible water-based polymeric solutions or polymer-salt solutions that remain separated by a discrete liquid-liquid interface when combined over critical concentrations (*80*, *81*). ATPSs were accidentally discovered by Beijerinck in 1896, but the first applications involving the use of ATPSs were demonstrated by Albertsson for the purification and isolation of various biomolecules such as proteins, DNA, and other materials (*82*). With the multitude of potential applications for ATPSs, characterization of these systems is necessary to determine the concentrations of each phase-separating species required to form a biphasic system. The composition at which phase separation occurs is dependent on the thermodynamic properties of the phase-separating solutions (*81*, *83–85*). In order to understand the ATPS formation, it is important to consider the free energy of the system:

$$\Delta G = \Delta H - T\Delta S$$

Where:

$\Delta G = change\ in\ Gibbs\ free\ energy$

$\Delta H = change\ in\ enthalpy$

$T = temperature$

$\Delta S = change\ in\ entropy$

The polymers will only phase-separate if $\Delta G > 0$. If $\Delta G < 0$, the process is spontaneous and the polymers will mix to form one solution with no distinguishable phases (*86–88*). Although several thermodynamic models have been developed to predict ATPSs formation, empirical approaches have also been used to determine the concentrations of polymers that give rise to single or two-phase systems (*89–91*). These empirical approaches are used to generate a phase diagram that delineates the concentrations at which ATPSs can form. Phase separation is influenced by a variety of factors including pH, molecular weight, polarity, viscosity and ionic content of the polymer/salt, and temperature (*68*, *76*, *77*). Several methods have been developed to determine polymer concentrations required for phase-separation, but the turbidimetric titration method and the cloud-point method are the most commonly used approaches (*81*, *91*, *92*). These methods rely on assessing the points at which the polymer solutions transition from miscible to immiscible phases and vice-versa. These points are represented on a phase separation diagram, as shown in Figure 1. Points above the curve give rise to immiscible phases, while points below the curve appear as a single miscible phase.

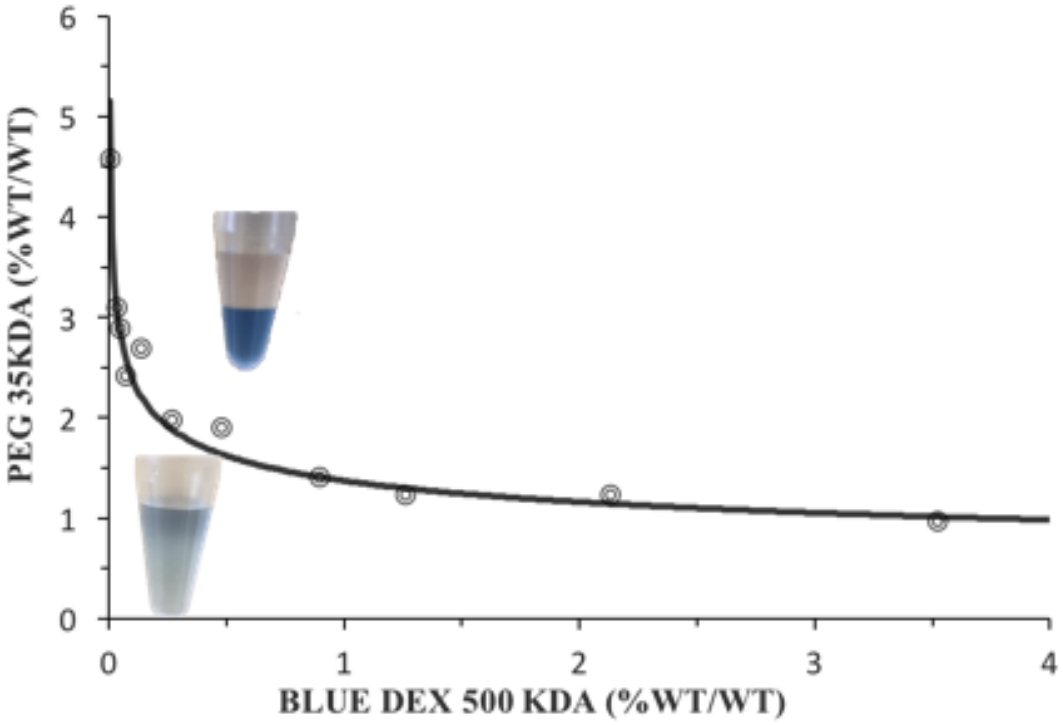

Figure 1 An example of a phase separation diagram of PEG 35 kDa - DEX 500 kDA (adapted from Agarwal et al., 2017)
X-axis represents concentrations of blue DEX in %wt, while y-axis represents the concentrations of PEG in %wt. Two known concentrations were combined to form an ATPS (tube above the curve). Small amount of buffer is gradually added to the phase-separating solution until the polymers can no longer phase-separate (tube below the curve). The process is repeated to generate the rest of the points on the curve. Any points above the curve gives rise to ATPSs, while the points below form a single-phase solution.

The most extensively studied biphasic system is comprised of poly(ethylene glycol) (PEG) and dextran (DEX) (*81*). PEG is a synthetic polymer that is synthesized from ethylene oxide and water, while DEX is a type of α-glucan that is mass produced from fermentation of sucrose-containing medium by *Leuconostoc mesenteroides* (*93*, *94*). PEG and DEX are the most widely used ATPS-forming polymers owing to their biocompatibility and cost-effectiveness. Moreover, these phase-separating polymers have low interfacial energy (γ_{12} ~ 0.003 mJm^{-2}), which allows the formation of stable patterns at a wide range of temperatures. Finally, the ATPS method uses high molecular weight PEG and DEX, which separate at low concentrations, and therefore these low concentrations of polymers do not exert any deleterious effects on cells (*81*, *95–98*).

Liquid-liquid phase-separation of DEX and PEG solutions has been used extensively for fractionation and isolation of DNA, virus, proteins, and antibodies. More recently, the partitioning of materials in the DEX-PEG system has been exploited for biopatterning of biomolecules and cells. This method takes advantage of the interfacial tension of PEG and DEX and the preferential distribution of reagents to one phase or the other to position biomolecules and particles such as cells in aqueous environments. ATPS-based cell biopatterning uses microliter volumes of DEX containing cells, which are dispensed onto a substrate coated with PEG solution using simple liquid handling devices such as micropipettes. The interfacial tension between the polymers confines the cells within the DEX droplets, allowing contact-free cell placement. Unlike other existing approaches that induce mechanical or thermal stresses on the materials undergoing deposition, ATPS is driven by ultralow interfacial tension that retains up to ~ 98% cell viability. In contrast to other biopatterning techniques, ATPS EBP is easy-to-learn, and does not require any

specialized equipment or training. It can pattern small volume of droplets (e.g., 0.5 µl) using simple readily available tools such as micropipettors. ATPS EBP can also be used to pattern bioparticles of various sizes, which may be difficult to achieve with other biopatterning techniques. Moreover, it is inexpensive and does not exert any deleterious effect on biomolecules or cells (*99*, *100*). However, in contrast to other biopatterning approaches, the printing speed of ATPS EBP may be slow.

Recent studies have demonstrated that ATPS biopatterning can be used to pattern cells into a range of configurations in vitro including cell islands, exclusion zones, co-cultures, heterocellular microarrays and cells patterned on a pre-existing monolayer. However, there have been only a few studies that have explored the effects of biphasic systems on cell growth, proliferation and differentiation. Here, I hypothesized that patterning keratinocytes in ATPS will enhance the proliferation and differentiation of keratinocytes in culture, which would be beneficial for skin tissue engineering.

1.8. Thesis Aims

The overall goal of this thesis is to explore the use of ATPS EBP to address key challenges in skin tissue engineering. While some tissues are sparsely populated, both the dermis and epidermis are cell-dense. Therefore, to recapitulate the epidermis and dermis, tissue constructs must have high cell densities. However, the limited availability of cells makes it challenging to fabricate large-scale tissue constructs with adequate cell densities to serve as replacements for damaged or diseased skin. Therefore, it is necessary to implement strategies that will efficiently use the limited cells that are available while still promoting

the growth and differentiation of cell dense constructs. In this thesis, I developed a cell delivery approach that utilizes ATPS EBP to efficiently deliver cells and promote their growth and differentiation in culture, as well as improve their engraftment on an acellular dermal matrix. Here, I hypothesized that biopatterning using ATPS EBP would tightly organize the cells, which would allow the cells to communicate effectively and promote the formation of intercellular junctions more rapidly than by dispersed cell seeding (Figure 2). In this work, I compared the ATPS EBP approach to the conventional cell seeding approach and examined beneficial effects on cell growth and engraftment on an acellular dermal matrix as a strategy for engineering a functional skin equivalent.

1.8.1. Aim 1

To identify the optimal concentration of ATPS-based bioink for cell patterning using a phase separation diagram and assess the effects of PEG and DEX concentration on cell morphology and stable ATPSs formation.

1.8.2. Aim 2

To apply ATPS EBP to efficiently biopattern human epidermal keratinocytes (HEK001) and examine the effects of ATPS EBP on cell viability, proliferation, and differentiation by biopatterning the cells on standard tissue culture plates and comparing them to the conventional dispersedly-seeded technique.

1.8.3. Aim 3

To demonstrate the application of ATPS EBP by biopatterning an array of HEK001 cells in discrete colonies on an acellular dermal matrix (DermGEN™) and assess cellular engraftment, proliferation, and differentiation of the stratum basale on DermGEN™ by comparing the biopatterned condition to the dispersedly-seeded condition.

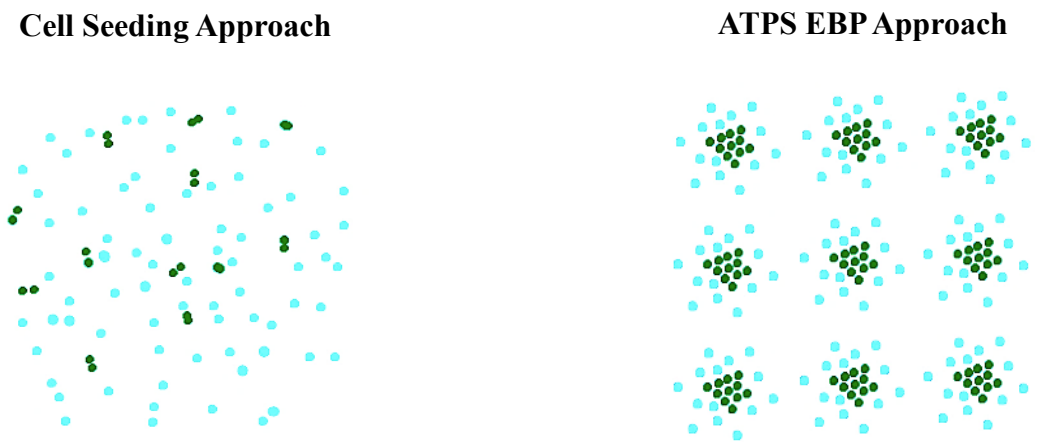

Figure 2 Cartoon representation of the cell delivery approaches.
Green cells represent the differentiated keratinocytes that have undergone contact inhibition of proliferation. The blue cells represent keratinocytes that are migrating and proliferating.

CHAPTER 2: MATERIALS AND METHODS

The content of this chapter has been previously reported (*101*) and has been described here again for readers. A few sections of this chapter have been adapted from a forthcoming manuscript. Below is a figure describing the methods used for each aim outlined in this thesis.

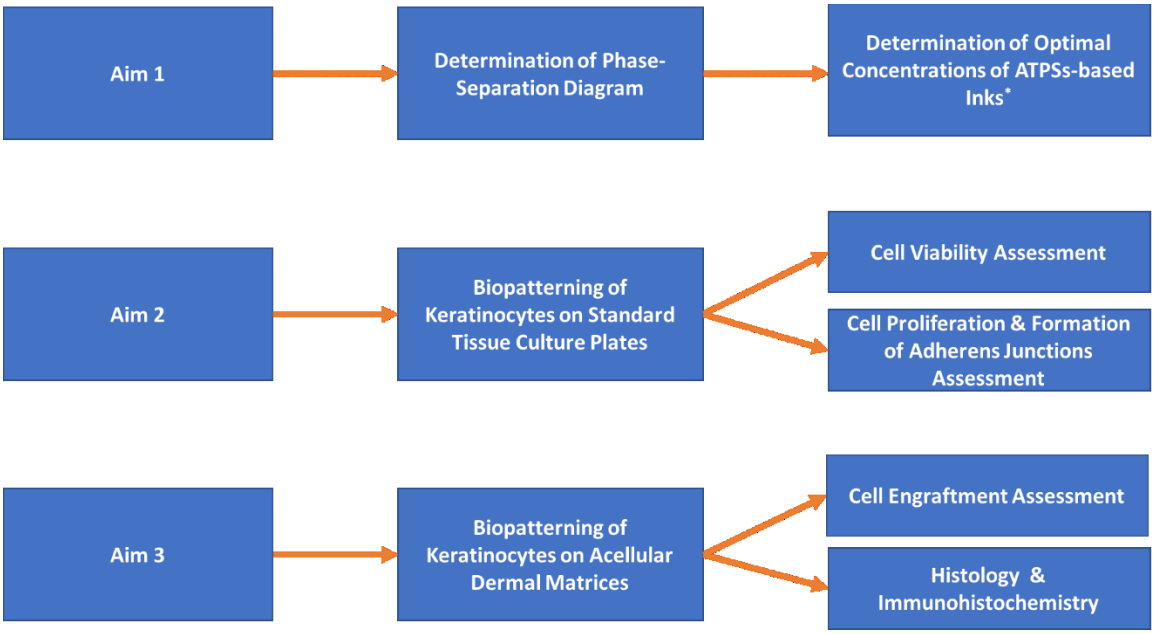

Figure 3 Specific methods used for each aim of the study.
In Aim 1, the phase-separation diagram of PEG 35kDa and 500 kDa was characterized, which was used to determine the optimal concentrations of ATPSs-based inks. In Aim 2, the cells were biopatterned on standard tissue culture plates and were compared to the dispersedly-seeded conditions. These samples were analyzed for cell viability, proliferation, and formation of adherens junctions. In Aim 3, cells were biopatterned on acellular dermal matrices. These cultures were analyzed for cell engraftment, cell proliferation and differentiation using immunohistochemistry. * denotes concentrations of ATPSs-based ink from Aim 1 was used for meeting the objectives of Aim 2 and Aim 3. Common methods are not included in this figure.

2.1. Cell Line

The human epidermal keratinocyte cell line (HEK001, ATCC® CRL-2404™) was purchased from ATCC®. The HEK001 cell line is derived from a 65-year-old male and expresses keratin 14, which is only present in proliferating basal-type keratinocytes. For my thesis work, I was interested in investigating the effects of my patterning technique on cellular proliferation, migration, and formation of a basal epidermal barrier. Therefore, I selected HEK001 basal-type keratinocytes for examining the effectiveness of my patterning technique and establishing a standardized model that could be applied to different cell lines.

2.2. Preparation of Polymer Systems

PEG 35 kDa and high-purity technical quality of DEX T500 kDa were obtained from Sigma-Aldrich and Pharmacosmos, respectively. Blue-DEX 500 kDa obtained from Sigma-Aldrich was also added to the DEX T500 kDa solution as a way to visualize the DEX droplets immersed in the PEG phase. PEG 35 kDa and DEX 500 kDa were dissolved in keratinocyte-serum free medium (K-SFM) composed of 1 % antibiotic antimycotic solution (Sigma-Aldrich). The tubes were left on a shaker overnight to ensure complete dissolution. Filter units (0.45 μm pore size, Sarstedt) were used to filter-sterilize the solutions. The concentrations of the polymers were calculated in % wt.

2.3. Determination of the Phase Separation Diagram

Determination of a phase-separation diagram (also known as the binodal curve) is important for optimizing the appropriate working concentrations of PEG 35 kDa and DEX 500 kDa for cell patterning. The phase-separation diagram is influenced by a variety of factors including polymer molecular weight, salt concentrations of the medium, pH, polymer polarity and viscosity (*81*). Since PEG and DEX are polydisperse (i.e, they consist of polymers chains of various lengths), it is necessary to characterize these systems for each batch of polymer obtained from the manufacturer prior to any application testing. Polydispersity may influence the phase-separation diagram as the molecular weight may vary batch-to-batch. The molecular weight of the polydisperse polymer is calculated as the average of the molecular weight of the chains present in the sample. There has yet to be any study that characterized the effects of specific salt contents present in K-SFM on the phase-separation diagram for PEG and DEX. Therefore, I decided to determine the binodal curve for PEG 35 kDa and DEX 500 kDa in K-SFM before optimizing polymer concentrations for HEK001 cell patterning.

Turbidimetric titration was used to determine the phase separation diagram of PEG 35kDa - DEX T500 kDa (*81*). In this method, stock solutions of 20% wt PEG 35kDa and 20% wt DEX T500 kDa were prepared in K-SFM, as described in Section 2.2. From the stock solutions, nineteen phase-separating solutions were prepared in 1.5 ml centrifuge tubes with the following initial concentrations: 19% PEG 35 kDa : 1% DEX 500 kDa, 18% PEG 35 kDa : 2% DEX 500 kDa, 17% PEG 35 kDa: 3% DEX 500 kDa, 16% PEG 35 kDa : 4% DEX 500 kDa , 15% PEG 35 kDa : 5% DEX 500 kDa, 14% PEG 35 kDa : 6% DEX

500 kDa, 13% PEG 35 kDa : 7% DEX 500 kDa, 12% PEG 35 kDa : 8% DEX 500 kDa, 11% PEG 35 kDa : 9% DEX 500 kDa, 10% PEG 35 kDa : 10% DEX 500 kDa, 9% PEG 35 kDa : 11% DEX 500 kDa, 8% PEG 35 kDa : 12% DEX 500 kDa, 7% PEG 35 kDa : 13% DEX 500 kDa, 6% PEG 35 kDa : 14% DEX 500 kDa, 5% PEG 35 kDa : 15% DEX 500 kDa, 4% PEG 35 kDa : 16% DEX 500 kDa, 3% PEG 35 kDa : 17% DEX 500 kDa, 2% PEG 35 kDa : 18% DEX 500 kDa, and 1% PEG 35 kDa : 19% DEX 500 kDa. The mass of each solution was recorded. Each tube was vortexed to ensure the solution appeared cloudy, which indicated the formation of an emulsion. A small volume (10- 20 µl) of K-SFM was then added to each tube. The tubes were vortexed and centrifuged at 1000 x g for 5 mins at 20 °C. After centrifugation, the tubes were observed for interface formation, which signified the formation of ATPSs. If an interface was observed, 10- 20 µl of K-SFM was added until the two-phase system transitioned to a one-phase solution and the interface was no longer visible after centrifugation. The final mass of each tube was recorded. The final concentrations of PEG and DEX were then calculated using the formula below:

$$C_i V_i = C_f V_f$$

Where:

$C_i = initial\ \ concentration\ of\ polymer$

$V_i = initial\ volume\ of\ polymer$

$C_f = final\ concentration\ of\ polymer$

$V_f = final\ volume\ of\ tube$

These concentrations were plotted to generate a phase separation diagram, which was used for identifying the combinations of PEG and DEX solutions suitable for cell patterning.

2.4. Determination of Optimal Concentrations of ATPSs-based Inks

Several combinations of PEG and DEX solutions were tested, as listed in Table 1. In order to determine the optimal concentrations of PEG and DEX for cell patterning, two types of ATPSs were considered: equilibrated and non-equilibrated systems. In equilibrated systems, the phase-separated solutions composed of PEG and DEX were prepared in 15 ml conical tubes. The tubes were centrifuged at 20°C for 20 mins at 3.0 rcf to equilibrate the polymers. After centrifugation, PEG and DEX solutions were separated in two different tubes, which were used for patterning. In non-equilibrated systems, pure PEG and DEX solutions were prepared in 15 ml conical tubes using the protocol outlined in Section 2.2. These tubes were not centrifuged prior to cell patterning. For each system, one-microliter droplets of cell-laden DEX were dispensed onto wells coated with PEG solution. These plates were analyzed for formation of stable ATPSs and uniform cell patterns.

2.5. Cell Culture

The human epidermal keratinocyte cell line (HEK001, ATCC® CRL-2404™) was cultured in K-SFM containing 2 mM L-glutamine and 10 ng/ml human recombinant epidermal growth factor (EGF, BioVision) in 100-mm culture dishes. The cells were passaged at ~60-70% confluence and were used for experiments before 30 passages, as described in the standard passaging protocols. The cells were maintained in a humidified incubator with 5% CO_2 and 37 °C. The cells were subcultured per ATCC instructions. Briefly, the cells were washed with 5 ml of 1X filter-sterilized phosphate buffered saline (PBS). Then, 2.0 ml of trypsin-EDTA (0.05% Trypsin/0.53 mM EDTA; Corning) was added to the cell

culture dish. The cell culture dish was placed in a humidified incubator at 37°C for ~5 - 7 mins to facilitate the trypsinization process. The cell culture dishes were gently tapped to detach any remaining adherent cells. Approximately 2.0 - 3.0 ml of Dulbecco's modified eagle's medium (DMEM) supplemented with 10% fetal bovine serum (FBS) and 1% antibiotics antibiotic solution was added to the cell suspension to deactivate the trypsin. The cell suspension was centrifuged at 20 °C for 5 min at 0.2 rcf and the supernatant was removed. The cell suspension was re-suspended in fresh cell culture medium and either re-plated to continue to grow the cells or used for experiments.

2.6. Biopatterning of Keratinocytes on Standard Tissue Culture Plates

HEK001 cells were printed in a colony pattern on standard 24-well tissue culture plates using the protocol described previously (Figure 4) (*101*). The PEG and DEX solutions were prepared using the procedure described in Section 2.2. Briefly, 500 µl of PEG 35 kDa solution was added to each well of a standard 24-well tissue plate (Figure 4A (i)). HEK001 cells were passaged as described in Section 2.5 and were re-suspended in 5.0% DEX. Cells were patterned at a concentration of 5000 cells/µl. A micropipette was used to dispense 1.0 µl cell-laden DEX ink in the center of each well of the culture plate prefilled with 5.0% PEG solution (Figure 4A (ii)). The steps mentioned above were repeated for the dispersedly-seeded condition, except these plates were agitated by gently shaking the plate to disperse the cell-rich DEX droplet across the well surfaces. In both conditions, the ATPSs-based bioink was used to isolate the effects of patterning condition versus the dispersedly-seeded condition. All plates were carefully stored in a 37 °C incubator to

facilitate cell attachment and growth. Plates were left undisturbed overnight. The following day (defined as day 1), polymers were discarded, and each well was washed with 250 µl of K-SFM three times. Next, 500 µl of fresh K-SFM medium supplemented with 1% antibiotic solution and 0.1 mM calcium (Ca^{2+}) was added to each well (Figure 4A (iii)). Calcium chloride was added to enhance intercellular junction formation. The plates were assessed for cell viability, cell proliferation, and formation of adherens junctions on days 1, 3, 7, and 14. As controls, microliter droplets of either cell-rich culture medium or cell-rich DEX were dispensed onto substrates coated with either PEG or medium (Figure 4B and 5C).

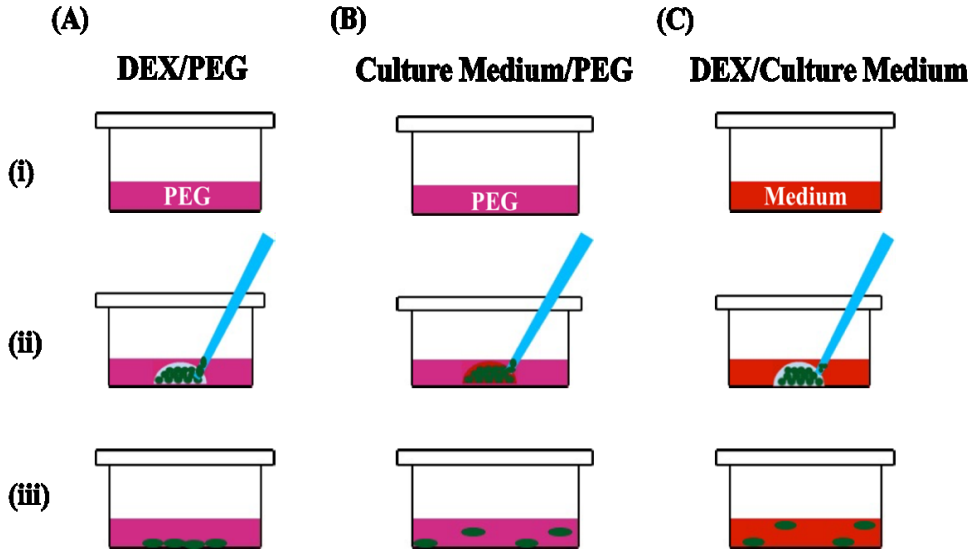

Figure 4 Cartoon representation of the ATPS EBP cell patterning protocol.
(A) depicts the ATPS EBP patterning protocol. In the ATPS EBP patterning procedure, (i) the surface of the well is coated with PEG. (ii) the cell-rich DEX droplet is dispensed onto a substrate coated with PEG solution. The plates are left in the incubator overnight. (iii) polymers are discarded the next day and are replaced with fresh K-SFM.
(B) and (C) shows the control conditions. (i) the well is coated with PEG (B) or cell culture medium (C). (ii) cell-rich medium droplet (B) or cell-rich DEX droplet (C) is pipetted to the well. (iii) the polymers are washed away and replaced by fresh K-SFM medium.

2.7. Cell Viability Assessment

Calcein-AM (C-AM, Biotium, 3 μM) and propidium iodide (PI, Sigma-Aldrich, 3 μM) staining was performed to assess the cell viability. C-AM was used to identify the living cells, which were stained green, whereas the PI was used to stain dead cells red. C-AM is a highly lipophilic molecule that permeates viable cells. Once inside cells, intracellular esterases hydrolyze C-AM to calcein, which produces a fluorescence signal at 530 nm upon excitation with blue light (*102*). PI, on the other hand, intercalates at guanine and cytosine base pairs of DNA and cannot enter living cells (*103*). C-AM and PI solution were prepared together in K-SFM. Next, 200 μl of the solution was added to each well and the plates were incubated for 10 mins in a humidified incubator at 37°C. Images were captured using a 2X objective lens on a Nikon Eclipse T1 epifluorescence microscope on days 1, 3, 7, and 14. Experiments were repeated three times and all the images were processed using Fiji image analysis software.

2.7.1. Image Analysis

Regions of interest (ROIs) were selected at the edge, mid-point, and center of each patterned colony. Similar regions were selected for the dispersedly- seeded conditions. The number of viable and dead cells were counted manually within each ROI using the cell counter option in Fiji. The percentage of viable cells were calculated and plotted as mean values ± SD.

2.8. Cell Proliferation and Formation of Adherens Junctions

2.8.1. Cell Proliferation Analysis

Proliferating cells were identified by Ki-67 immunofluorescence. Ki-67 is a proliferation marker that is found in the nucleus during the cell cycle (*104*). Both conditions were analyzed for the presence of proliferating cells on days 1, 3, 7, and 14. At each time point, the cells were fixed by adding 200 µl of 3.7% formaldehyde (Sigma-Aldrich) to each well for 10 mins. Each well was then washed three times with 1X PBS. Since Ki-67 is an intracellular marker, cells were permeablized with 25% Triton X-100 (Sigma-Aldrich) in PBS with Tween 20 (PBST) for 10 mins at room temperature. Each well was washed three times with 1X PBS for 5 mins per wash. Cells were then blocked with 1 % bovine serum albumin (BSA) in PBST for 30 mins at room temperature. All samples were then incubated in primary antibody, Ki-67/MKI67 Antibody (8D5) (NBP2-22112, Novus Biologicals, 1:500) overnight. HiLyte 488-conjugated anti-mouse IgG (NB710-40671, Novus Biologicals, 4.5 µg/ml) was applied as a secondary antibody for an hour to detect the fluorescent signal. Once the cultured plates were washed three times with PBS, bisBenzimide Hoechst 33342 trihydrochloride (B2261-25MG, Sigma-Aldrich, 1:1500) was applied as a counterstain for 10 mins. Again, all the experiments were replicated three times and images were acquired at 10X magnification using a Nikon Eclipse T1 epifluorescence microscope.

Image Analysis

Fiji was used to calculate the proliferation index. Like the cell viability assessment, three ROIs were selected for each image. Within each ROI, Ki-67 positive cells (stained in green) and the total number of cells (stained in blue by Hoechst) were manually counted using the cell counter option. A proliferation index was then calculated using the formula given below and plotted as mean values ± SD.

$$Proliferation\ index = \frac{Ki-67\ positive\ cells}{total\ number\ of\ cells} \times\ 100\%$$

2.8.2. Formation of Adherens Junctions

The formation of adherens junctions was detected by E-cadherin immunofluorescence. E-cadherins are the major transmembrane proteins in adherens junctions that mediate cell-cell contact (*105*). Briefly, all culture plates were fixed in 3.7% formaldehyde for 10 mins at room temperature. Each well was washed three times with PBS. The samples were then blocked in 1% BSA in PBS for 30 mins at room temperature, and E-cadherin Antibody (AF748, Novus Biologicals, 1:500) was applied to the samples overnight. The primary antibody was removed the next day and each well was washed three times with PBS for 5 mins. Finally, the secondary antibody, Dylight-488-conjugated donkey anti-goat IgG (NBP1-72843, Novus Biologicals, 1:2000), was used for detecting the presence of E-

cadherin. Cell nuclei were counterstained with bisBenzimide Hoechst 33342 trihydrochloride (B2261-25MG, Sigma-Aldrich, 1:1500). All plates were imaged at 10X magnification with the Nikon Eclipse T1 epifluorescence microscope.

Image Analysis

The relative expression of E-cadherin was determined using ImageJ. Three ROIs were selected within each well of the plates and were imaged at 10X magnification. Bernsen auto local threshold was used to process all the images. Finally, the percent area fraction was measured from the resulting images to detect the presence of E-cadherin in each condition in arbitrary units (AU). These values were then plotted as mean values ± SD.

2.9. Biopatterning of cells on Acellular Dermal Matrices

To demonstrate the potential application of the ATPS EBP technique to skin reconstruction, HEK001 cells were biopatterned on DermGEN™ (2 cm x 2 cm, DeCell Technologies). DermGEN™ is derived from donated human skin that has been processed to remove any immunogenic components, while retaining the native structure of the dermal component of the skin. A 3 x 3 array of HEK001 cells were biopatterned in colonies on DermGEN™ using the procedure mentioned in section 2.6. The cells were dispersedly-seeded in ATPS on DermGEN™ by gently shaking the plate to disperse the cells across the surface of DermGEN™. All cultures were monitored for cell engraftment, cell proliferation, and formation of adherens junctions on days 1, 3, 7, and 14. All the experiments for both patterned and dispersedly-seeded conditions were performed on treated plates.

2.10. Cell Engraftment Assessment

RealTime-Glo™ MT cell viability assay (Promega) was used to assess cellular engraftment on DermGEN™ in real-time. RealTime-Glo™ MT cell viability assay, a non-lytic cell assay, measures the reduction potential of cells. It contains NanoLuc Luciferase (also known as NanoLuc® enzyme) and MT cell viability substrate, which are added to cell culture medium. The MT cell viability substrate diffuses into living cells and gets reduced to NanoLuc substrate. Once the substrate is released into the medium, the substrate gets reduced by the NanoLuc Luciferase enzyme to produce a luminescent signal. The luminescent signal is directly correlated with number of living cells. The dead cells lack the capability to reduce the MT cell viability substrate to NanoLuc substrate. In order to measure cellular engraftment on DermGEN™, 3.0 µl of the 100x MT cell viability substrate and 0.6 µl of 500x NanoLuc® enzyme were added to each well containing 300 µl of medium. The plates were stored in an incubator for an hour. Images were taken using Azure Biosystems imager. Finally, the bioluminescent signal was quantified using a FilterMax F5 plate reader. The above steps were repeated on days 1, 3, 7, and 14 to monitor cellular engraftment in real-time. This experiment was replicated three times and data were represented in relative light units (RLU) as mean values ± SD.

2.11. Histology and Immunohistochemistry

All DermGEN™ samples were fixed in 10% neutral buffered formalin (NBF) for 24 hours and were washed twice with 70% ethanol. These samples were then embedded in paraffin and 5 µm sections of DermGEN™ samples were cut for immunohistochemistry. Hematoxylin and Eosin (H&E) were applied to the sections of DermGEN™ to stain the

nucleus and cytoplasm, respectively. Additional sections were used to evaluate cell proliferation and differentiation on DermGEN^{TM}. As mentioned earlier, Ki-67 and E-cadherin were used to examine cell proliferation and differentiation, respectively. All the sections were deparaffinized through two changes of xylenes (histological grade, Sigma-Aldrich) and a change of 1:1 xylenes: 100% ethyl alcohol anhydrous (Sigma-Aldrich) for 3 mins. The sections were gradually hydrated through graded alcohols in the following order: two changes of 100% ethyl alcohol (anhydrous) for 3 mins, two changes of 95% ethyl alcohol for 3 mins each, 90% ethyl alcohol for 3 mins, 70% ethyl alcohol for 3 mins, and 50% ethyl alcohol for 3 mins. Finally, all the sections were washed in dH_2O for 5 mins. The next step was to retrieve antigens, which may have been masked by chemical modifications by the NBF. The deparaffinized and hydrated sections were placed in 10 mM sodium citrate buffer for either 15 min (E-cadherin) or 20 min (Ki-67) at ~99°C. The sections were then washed three times in 1X PBS for 5 mins/wash. All the sections that were being stained for E-cadherin were blocked in 1% BSA in PBS, while the sections for Ki-67 staining were blocked in 1 % BSA in PBST for 30 mins at room temperature. E-cadherin Antibody in PBS (1:500) and Ki-67/MKI67 Antibody in PBST (1:200) were applied to the sections and were incubated overnight. The sections were washed three times with PBS for 5 mins/wash. The sections were incubated in 488-conjugated anti-goat IgG secondary antibody (1:1500) and a 555-conjugated anti-mouse IgG1 (γ1) secondary antibody (SAB4600302-125UL, Sigma-Aldrich, 7 μg/ml) for an hour for detection of E-cadherin and Ki-67, respectively. The samples were then washed again with 1X PBS. As a counterstain, Hoechst 33342 was applied to the sections for 10 mins, and the sections were washed three times with 1X PBS. All the sections were imaged at 10X using Nikon Eclipse

T1 epifluorescence microscope. Brightfield microscopy was used to image the H&E sections at 20X magnification.

2.12. Statistical Analysis

Two-way analysis of variance (ANOVA) and Tukey multiple comparison test was performed to compare the impacts of ATPS EBP and dispersedly-seeded approach on cell viability, proliferation and differentiation over several days. Data are represented as mean ± SD. Statistical significance was defined as *$p<0.05$.

CHAPTER 3: RESULTS & DISCUSSION

3.1. Characterization of ATPS-based Inks for Cell Delivery

3.1.1. Rationale

The first goal of my thesis work was to determine a novel bio-ink for EBP and to optimize the concentrations of the selected bio-ink for cell delivery. The current bio-inks used for EBP are unable to print on a wet substrate without a loss of pattern fidelity. Moreover, patterning cells in air can cause the cells to dehydrate, affecting their viability. Attempts have also been made to print cells on moist substrates to prevent cellular stress. However, the subsequent addition of media required for cell attachment washes away any pattern. Therefore, it is important to determine a novel bio-ink that would maintain the pattern fidelity when deposited on a wet substrate and provide a nutrient-rich environment to the cells. To do so, I chose an ATPS as a bio-ink for EBP. ATPSs are comprised of two or more polymers that separate when combined over critical concentrations. One of the most extensively studied biphasic systems is PEG and DEX. PEG and DEX are biocompatible, cost-effective, and easy to handle. Patterned cells can retain up to 98% of cell viability in this ATPS (*81*, *95*). Furthermore, the interface between PEG and DEX has ultralow interfacial tension, making it easy to produce stable and uniform droplet patterns. These features would make the technique more accessible and encourage researchers to use the ATPS EBP technique for optimizing cell-cell and cell-ECM interactions and producing more physiologically relevant tissue models.

My next step was to determine the optimal concentrations of ATPSs for cell delivery. To achieve this, I had to characterize the binodal curve for PEG 35 kDa and DEX 500 kDa, which delineates the concentrations at which ATPSs form. Although several phase-separation diagrams have been reported in the literature previously, the phase separation properties of the polymers can be affected by several factors including, but not limited to, ionic content of the medium, molecular weight, and pH (*81*). No previous studies have optimized the concentrations of ATPSs-based ink for HEK001 patterning. Therefore, characterization of this system prior to its application was necessary. Based on the phase-separation diagram of PEG 35 kDa and DEX 500 kDa, several combinations of PEG and DEX were assessed for formation of stable ATPSs and uniform cell patterns.

NOTE: Portions of this section has been adapted from an MRS Advances publication (Please see Appendix A) (*101*).

3.1.2. Optimization of Polymer Concentrations for ATPS EBP of HEK001 Cells

To optimize the appropriate working concentrations of PEG and DEX, a binodal curve was constructed. Since a wide range of factors (such as the polydispersity of PEG and DEX and the variation of ionic content in the customized cell culture medium) can have an influence on the phase separation diagram, it is important to experimentally determine this diagram (*81*). There are several methods that can be used to construct the binodal curve, but the turbidimetric titration method is one of the most commonly used approaches. This method relies on generating a series of ATPSs forming solutions, and then adding solvent to the

polymer mixture until the solutions do not phase separate. Using the turbidimetric titration method, the binodal curve of PEG 35 kDa and DEX 500 kDa was generated (Figure 5) (*81*). Any points above the curve signify combinations of PEG and DEX that can be utilized to form phase-separated solutions, while the combinations of PEG and DEX below the curve appear as one solution.

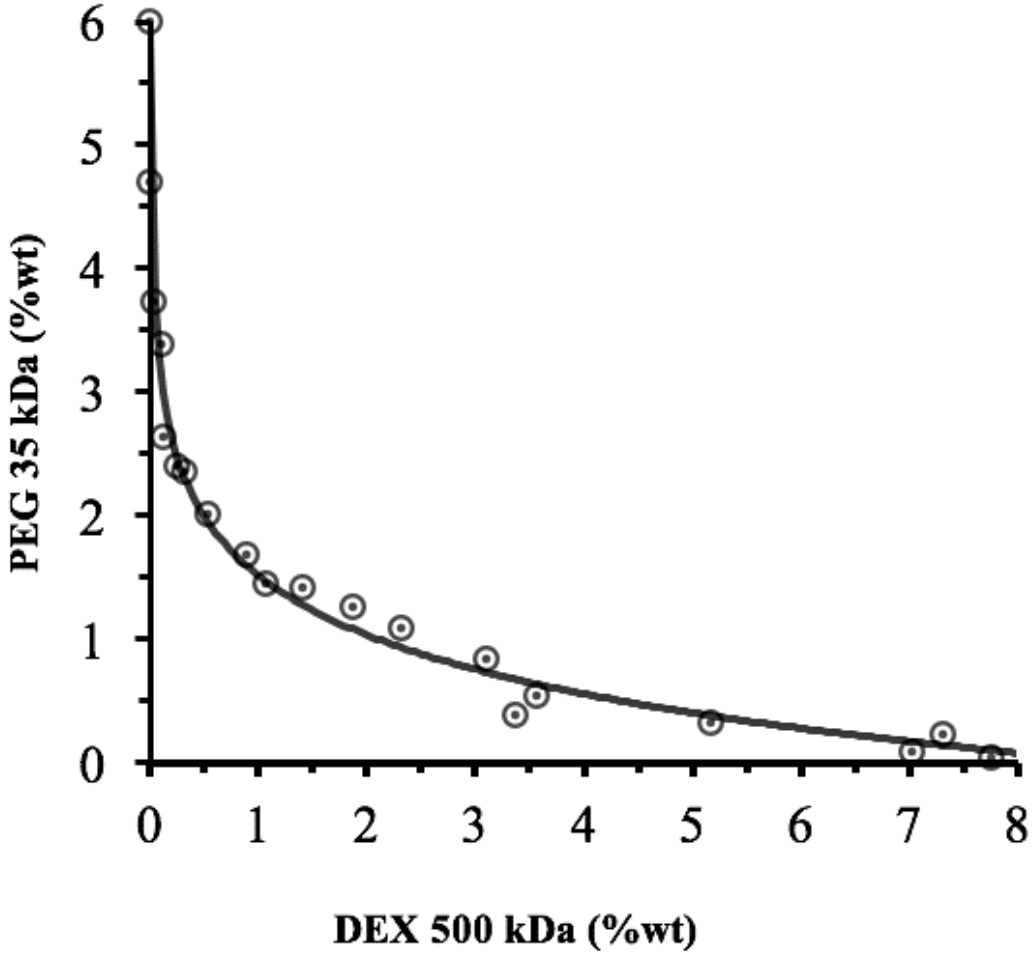

Figure 5 Phase separation diagram of PEG 35 kDa and DEX 500 kDa determined using the turbidimetric titration method.
The Y-axis represents the concentration of PEG 35 kDa in % wt, while the concentrations of DEX 500 kDa in % wt are represented on the X-axis.

Based on the phase separation diagram shown in Figure 5, various combinations of pure solutions of PEG and DEX were tested (as listed in Table 1). Once the polymer solutions were equilibrated with respect to each other, some of the formulations did not form stable patterns and were not able to maintain colony patterning (as indicated by an X mark in Table 1). It was observed that 2% PEG : 10% DEX and 14%PEG : 0.6% DEX did not form stable patterns, and therefore were not used for cell patterning. When cells were patterned using the 14% PEG : 0.6% DEX formulation, cells appeared very rounded, which could have been due to the effects of PEG on cells at higher concentrations. Previous studies have reported that low molecular weight PEG is toxic to cells and can cause disruption of plasma membrane at high polymer concentrations (*99*, *106*, *107*). Therefore, I selected the ATPSs combination based on the lowest concentration of PEG to avoid or minimize any deleterious impact of PEG on cell viability. Although 7.5 % PEG : 6.6 % DEX showed stable pattern formation and did not have an impact on cell morphology, this formulation was not considered as a potential candidate for further optimization due to the higher concentration of PEG (as shown in Table 1).

Table 1 Assessment of ATPS Formulations for Cell Patterning
Formulations that resulted in rounded cell morphology or unstable pattern formation are represented by X, while the combination of ATPS that formed stable pattern and retained normal cellular morphology are represented by ✓.

ATPS Formulations	Stable Pattern Formation	Cell Morpholoy
2% PEG : 10% DEX	X	✓
5.0% PEG : 4.0% DEX	X /✓	✓
5.0% PEG : 4.5 % DEX	X /✓	✓
5.0% PEG : 5.0 % DEX	✓	✓
5.0% PEG : 5.5 % DEX	✓	✓
7.5 % PEG : 6.6 % DEX	✓	✓
14%PEG : 0.6% DEX	X	X

Since 5.0% PEG : 4.0% DEX, 5.0% PEG : 4.5%, DEX 5.0% PEG : 5.0% DEX, 5.0% PEG : 5.5% DEX showed promising preliminary results (Table 1), these concentrations were further optimized using two different ATPS formats (equilibrated systems and non-equilibrated systems), as shown in Figure 6. In equilibrated systems, PEG and DEX were equilibrated with respect to each other. After equilibration, the two phases were collected in separate tubes, which were used for cell patterning. Non-equilibrated systems were comprised of pure solutions and were directly used for cell patterning. Both equilibrated and non-equilibrated systems were assessed for formation of stable ATPS interfaces and

uniform patterns, and showed very similar results (as can be seen in Figure 6). Thus, the non-equilibrated systems were selected for subsequent investigation of cell delivery approaches due to the relative simplicity of the procedure.

Out of four combination selected for cell patterning, both 5.0% PEG : 5.5% DEX and 5.0% PEG : 5.0 % DEX resulted in formation of uniformly patterned colonies along with stable ATPS interfaces after patterning (indicated by arrows in Figure 6). Interestingly, I also observed that 5.0% PEG : 4.5% DEX and 5.0% PEG : 4.0 % DEX resulted in inconsistent pattern formation. These concentrations did not form stable ATPSs after patterning. This effect is most likely seen due to interfacial tension properties of the phase-separating polymers, but could also result from gradual loss of phase separation as the DEX droplet equilibrates with the surrounding PEG solution (*108*). Since both 5.0% PEG : 5.5% DEX and 5.0% PEG : 5.0 % DEX showed promising results, I selected 5.0% PEG : 5.0 % DEX for ATPS EBP because it uses lower amounts of polymers. In addition, low concentrations of polymers do not alter the media composition as much and are less likely to interfere with cell adhesion to the substrate (*108*).

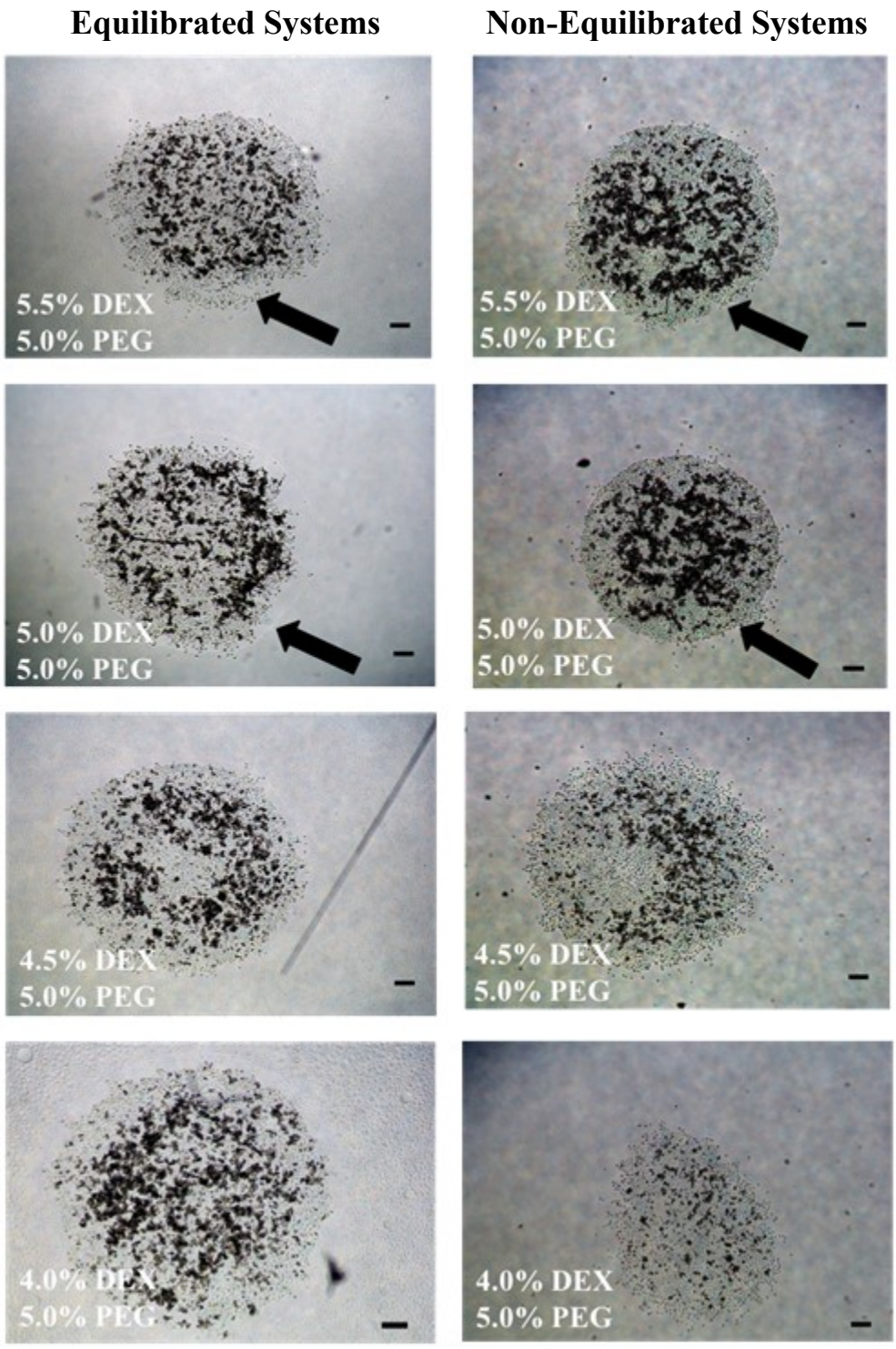

Figure 6 Representative images (2X) of equilibrated and non-equilibrated ATPS formulations for cell delivery.
Cells were printed at a concentration of 5000cells/µl. Arrow indicates stable ATPSs formation 24 hours post patterning. Scale bars = 100 µm.

Additional experiments not detailed in this thesis were performed to assess the impact of cell density on the ATPS formulation used for cell patterning. Cell densities ranging from 2,500 to 30,000 cells per microliter were investigated. I wanted to select a combination of ATPS formulation and cell density that would result in uniform pattern with sufficient number of cells covering the substrate surface underneath the DEX droplet. I discovered that cell densities above 10,000 cells per microliter resulted in poor cell attachment. Further, excess cells tended to collect at the interface. This phenomenon can be explained by thermodynamic properties of the ATPSs. A study conducted by Tavana et al. demonstrated that partition of cells in ATPS relies on the interfacial tension of the polymer as well as the contact angle (θ). The cells will only partition to the DEX droplet and form a stable pattern – if the interfacial tension is small and ATPS formulation are able to satisfy the following condition: $0<\theta<90°$ (*109*). When 2,500 cells per DEX droplet were dispensed in the PEG phase, the cells partitioned to the DEX droplet, but were unable to fully cover the surface beneath the DEX droplet. Finally, when 5000 cells were patterned in the PEG phase, cells were able to completely cover the substrate underneath the DEX droplet. Thus, 5000 cells per DEX droplet was selected as an optimal cell density for subsequent investigation of cell delivery approaches.

3.1.3. ATPSs as a Potential Ink for EBP

The next step was to investigate if ATPSs could be used to maintain pattern fidelity on a substrate immersed in culture medium (CM). This was achieved by pipetting a droplet of cell-laden 5.0% DEX onto a tissue culture plate immersed in 5.0% PEG solution at a concentration of 5000cells/µl. As shown in Figure 7A, a patterned colony is observed when both PEG and DEX are used. This is because of the interfacial tension between the PEG

and DEX solution, which confines the cells to the DEX droplet (*99*). As controls, cell-rich PEG and cell-rich DEX droplets were also dispensed onto a well coated with CM (Figure 7B and 7C). As expected, the cells in both conditions were non-uniformly distributed across the well surfaces and were not able to maintain pattern fidelity. Finally, the cells were deposited in CM. As expected, cells in CM were also unable to maintain pattern fidelity (Figure 7D). These results suggested that both PEG and DEX are required for pattern formation. The results also supported the hypothesis that pattern fidelity is maintained due to the phase-separating properties of the polymers rather than the effects of the viscosity of the polymers.

Next, C-AM and PI staining was performed to examine the effects of polymers on cell viability. The qualitative results suggested that the cell viability was quite high across all the conditions (indicated by C-AM staining in Figure 7). There were very few dead cells observed in the cultures, represented by PI staining, which was consistent with previous observations. These results demonstrated that 5.0% PEG and 5.0% DEX were non-toxic to cells and had no discernable impacts on cellular activity.

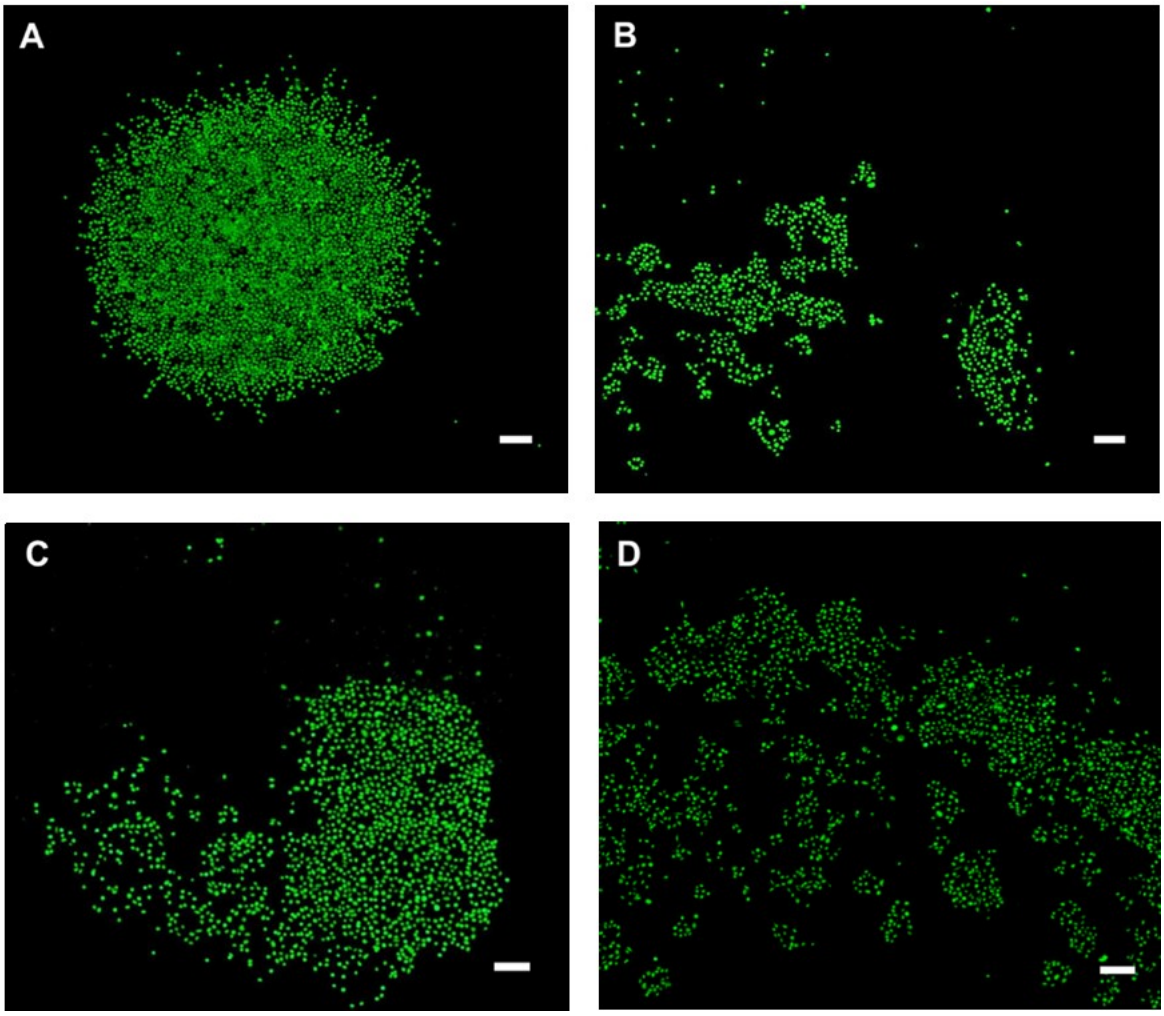

Figure 7 Representation images (2X) of cells patterned in ATPS, PEG-alone, DEX-alone, and CM.
Cell were patterned in colony patterns using PEG/DEX (A), PEG/CM (B), DEX/CM (C), and CM (D). C-AM (green)/ PI (red) stain was used to identify living and dead cells, respectively. Scale bars = 100 μm.

In this section, I presented a novel bio-ink for EBP. I also characterized the ATPS systems along with the optimal cell density number for patterning of HEK001 cells. Stable pattern formation and uniform patterns were observed at non-equilibrated combination of 5.0 % PEG and 5.0% DEX at a cell density of 5000 cells/µl. ATPS EBP also showed excellent cell viability. Furthermore, it allowed patterning of cells in polymer solutions comprised mostly of cell culture medium to ensure that cells were able to maintain their patterns in a nutrient-rich environment, overcoming a major limitation of the conventional biopatterning techniques.

Many patterning techniques (e.g., LaBP and IBP) have been used to localize cells, but these approaches require complex instrumentation and highly specialized training, which may not be accessible to life scientists (*68*, *103*). The cost of these highly-specialized techniques is a major limitation. On the other hand, my ATPS EBP is simple, contact-free, affordable, and can be performed using tools such as micropipettor that are readily available in life science laboratories. Of course, it is possible to produce high-throughput, complex patterns by implementing sophisticated technologies such as the liquid handling robots and acoustic droplet ejection (ADE) (*95*, *110*). For instance, Fang et al. generated multiplexed pattern of cocultures by combining acoustic droplet ejection with ATPS patterning to investigate the response of a signaling pathway that mediates cancer metastasis.

Although ATPS EBP is efficient in patterning a wide variety of biomolecules, there are a few factors that need to be considered to generate consistent patterns. To generate patterns of consistent droplet volumes, the pipette tip used for dispensing the DEX droplet should

be changed after the droplet has been dispensed onto a substrate. Tilting the tissue culture plate or shaking the plate vigorously should be avoided once the DEX droplets are dispensed onto a plate coated with PEG solution to minimize droplet disruption. Therefore, extra care must be taken if the plates are moved being back and forth from the incubator.

Despite these technical issues, ATPS EBP patterning technology has shown significant promises in a wide variety of applications (*111*). Recently, Tavana et al. has explored the properties of ATPS EBP for investigating the effects of microenvironmental interactions on cell growth and differentiation. Their group demonstrated enhanced neuronal differentiation when mouse embryonic stem cells (MESCs) were printed on PA6 stromal cells (*109*, *112*). Since ATPSs were able to improve neuronal differentiation, I thought I could potentially use this unique feature of ATPS EBP to improve growth and differentiation of keratinocytes and address a few key challenges in skin tissue engineering, as discussed in section 3.2.

3.2. Biopatterning of Keratinocytes on Tissue Culture Plates

3.2.1. Rationale

In section 3.1., I presented a promising novel bio-ink for EBP that takes advantage of the interfacial tension between phase-separating polymers to pattern cells onto a wet substrate. Recent studies have shown that this ATPS EBP technology is capable of improving cell growth and differentiation in culture. It has also allowed researches to investigate the effects of homotypic and heterotypic interactions on cellular behavior. Therefore, my next step was to use this interesting feature of ATPS EBP and apply it to biopattern

keratinocytes for skin tissue engineering. As outlined in chapter 1, epidermal reconstruction approaches use CEA sheet composed of autologous keratinocytes to restore the epidermis. However, it takes weeks for the cells to grow to form stable sheets for transplantation. Alternatively, cell seeding and cell spraying methods have been explored for epidermal reconstruction. These approaches, however, lack precision and are unable to recreate the complexity of the epidermis. Moreover, the limited availability of autologous keratinocytes makes it difficult to fabricate a cell-dense tissue construct in an appropriate time frame. Therefore, it is necessary to implement strategies that will enhance cell expansion and differentiation in culture.

I utilized the ATPS EBP cell delivery approach to efficiently biopattern cells at a target site. Here, I hypothesized that the tight organization of cells in the ATPS-based ink would promote homotypic and heterotypic interactions appropriate for cell growth and differentiation. Thus, the ATPS EBP approach was used to pattern HEK001 cells in colonies to better support their growth (*99*, *113*). The effectiveness of the ATPS EBP cell approach was determined by comparing two conditions: the patterned condition and the dispersedly-seeded condition (method outlined in section 2.6). Both conditions were assessed for cell viability, proliferation, and formation of adherens junctions.

NOTE: Portions of this section has been adapted from an MRS Advances publication (please see Appendix A) (*101*).

3.2.2. Cell Viability Assessment

The utility of ATPS EBP for skin tissue engineering was examined by biopatterning HEK001 cells in colonies and comparing them to cells in dispersedly-seeded conditions. The ATPS EBP cell delivery approach allows patterning of cells in a range of configurations *in vitro* including cell islands, exclusion zones, co-cultures, heterocellular microarrays and cells patterned on a pre-existing monolayer (*96*, *99*, *109*). To select the appropriate configuration for biopatterning in my study, the growth patterns of keratinocytes were considered. Although the mechanism is not clearly understood, previous studies have reported the colony-forming ability of keratinocytes (*113*, *114*). It has also been speculated that colony formation and migration of keratinocytes plays an important role in re-epithelialization of wounds (*115*). Moreover, the colony-forming ability of keratinocytes is observed when the cells are cultured on tissue culture plates. Therefore, to better mimic the natural growth environment of keratinocytes, I selected an ATPS printing procedure that allows the cells to be patterned in discrete colonies. I hypothesized that patterning cells in their normal growth pattern would result in improved communication between the cells, thereby improving the growth and differentiation properties of cells in culture. Using 5.0% PEG : 5.0% DEX, cell-laden DEX droplets were deposited onto a substrate coated with PEG at a concertation of 5000 cells per microliter. As a control, 5000 cells per microliter were dispersedly-seeded in ATPS. These cultures were assessed for cell viability over 14 days to evaluate the efficiency of ATPS EBP cell delivery over the pre-existing cell seeding approach (Figure 8).

As shown in Figure 8, C-AM/PI was used to examine the living cells and dead cells in both conditions, respectively. The C-AM/PI assay revealed that the patterned conditions had higher cell viability than the dispersedly-seeded condition across all days (Figure 8). These qualitative results also demonstrated that higher numbers of dead cells were observed at early time points for the dispersedly-seeded conditions as compared to the patterned conditions. Similar patterns of cell viability were observed for both conditions on days 7 and 14.

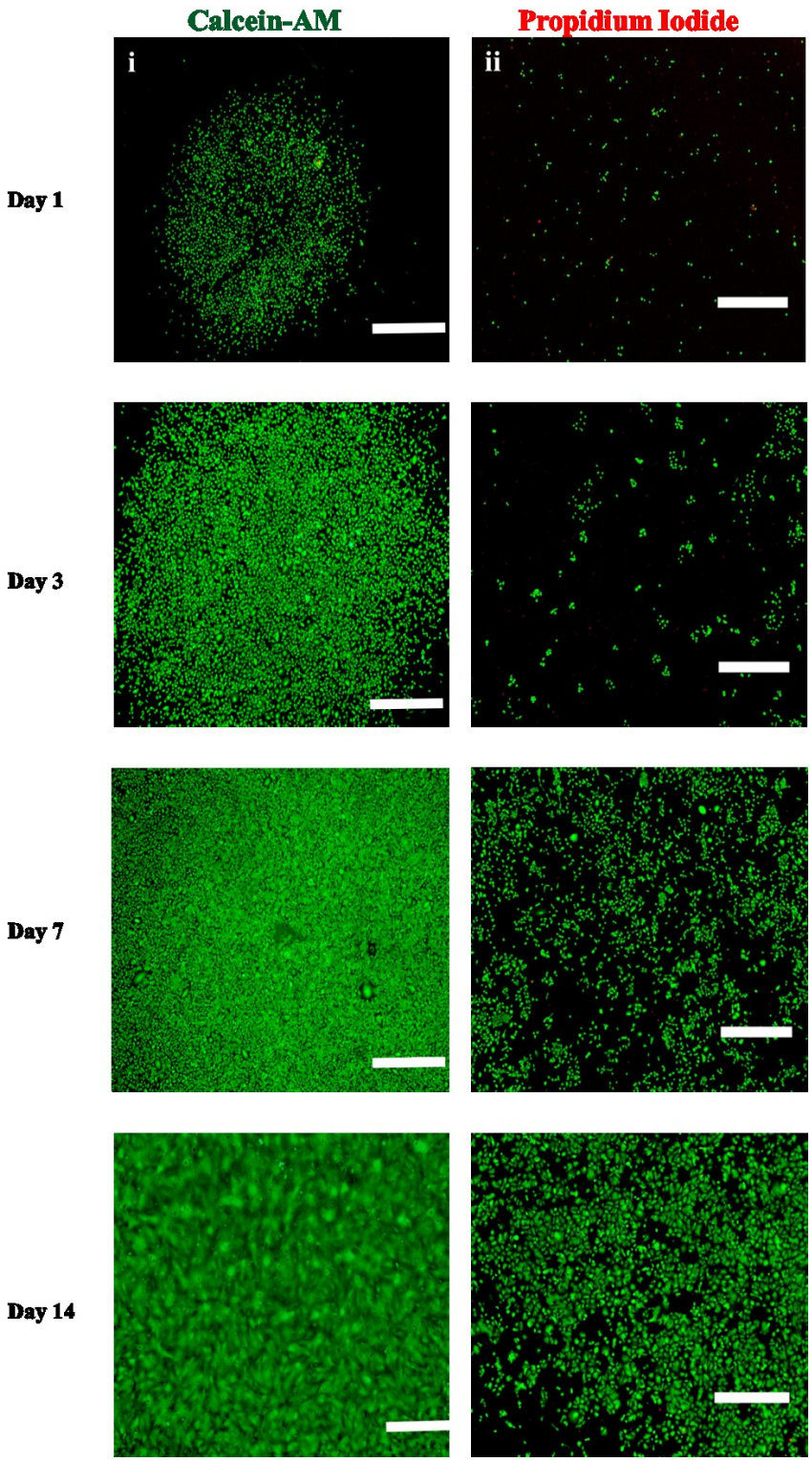

Figure 8 Cell viability assay.
Representative images (2X) of calcein-AM (green) and propidium iodide (red)-stained HEK001 cells in both patterned (i) and dispersedly-seeded (ii) conditions. Scale bars = 500 μm.

The cell viability data were further quantified in Fiji. Based on the results in Figure 9, the patterned conditions demonstrated cell viability of ~95%, whereas the dispersedly-seeded condition only had a cell viability of ~56% on day 1. A similar trend for cell viability was observed for both conditions on day 3 of culture. Low viability in early days for the dispersedly-seeded condition is most likely seen because of the lack of cell-cell contact. The cells are unable to communicate with each other via juxtacrine (contact-dependent) signaling, which affects the autocrine (signaling molecule binding to the receptor of the same cell) signaling pathway. For example, it has been previously reported that keratinocyte proliferation and migration are mediated by the epidermal growth factor receptor (EGFR), which gets activated via autocrine and juxtacrine signaling (*116–119*). Thus, it is important for keratinocytes to communicate with their neighbouring cells and the environment to direct epidermal renewal.

Interestingly, after 7 days of culture, the cell viability in the dispersedly-seeded condition improved to ~92%, which is close to the viability achieved by cells in the patterned condition (~99%). Similarly, high cell viability was observed in both conditions for day 14. Although viability was initially low in the dispersedly-seeded condition, enough cells survived and were able to proliferate, restoring viability by establishing some cell-cell contacts. The results of the cell viability assay suggest that patterning cells in colonies using ATPS EBP allows cells to more rapidly establish communication with neighbouring cells compared to the cells in the dispersedly-seeded condition, resulting in improved cell viability at early time points and higher efficiency of cell production.

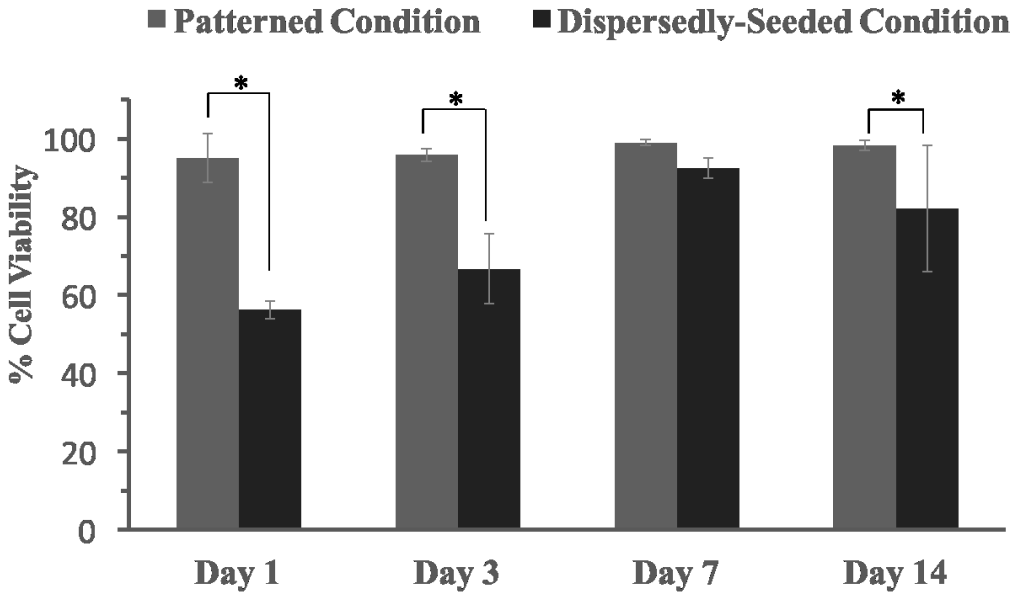

Figure 9 Quantification of calcein-AM and propidium iodide expression in HEK001 cells.
The Y-axis represents % cell viability of total cells and the X-axis represent the number of days. Values are the mean of three independent experiments and error bars represent the standard deviation.

3.2.3. Assessment of Cell Proliferation and Formation of Adherens Junctions

Next, the growth of the patterned colonies was monitored over 14 days. As shown in Figure 10, the size of the colonies increased over time, which can be seen by a gradual decrease in the scale bar. By day 14, the colonies were densely packed. When observed under the microscope, it appeared that the cells in the middle of the colony might be beginning to stratify by day 14. This observation is expected because keratinocytes display contact inhibition of proliferation (*120*, *121*). In contact inhibition, when cells are in close proximity with respect to one another, they cease to proliferate and undergo alterations to

form more mature or differentiated cell types. Therefore, contact inhibition is an important characteristic of differentiated tissues. Although several mechanisms have been proposed for contact inhibition, cell-cell contact mediated by E-cadherin and ß-catenin seems to be important. E-cadherin is important for formation of adherens junctions, while ß-catenin plays a key role in both cell proliferation and adherens junction formation. Although the mechanism is not clearly understood, E-cadherin is believed to downregulate the proliferative genes (*122*, *123*).

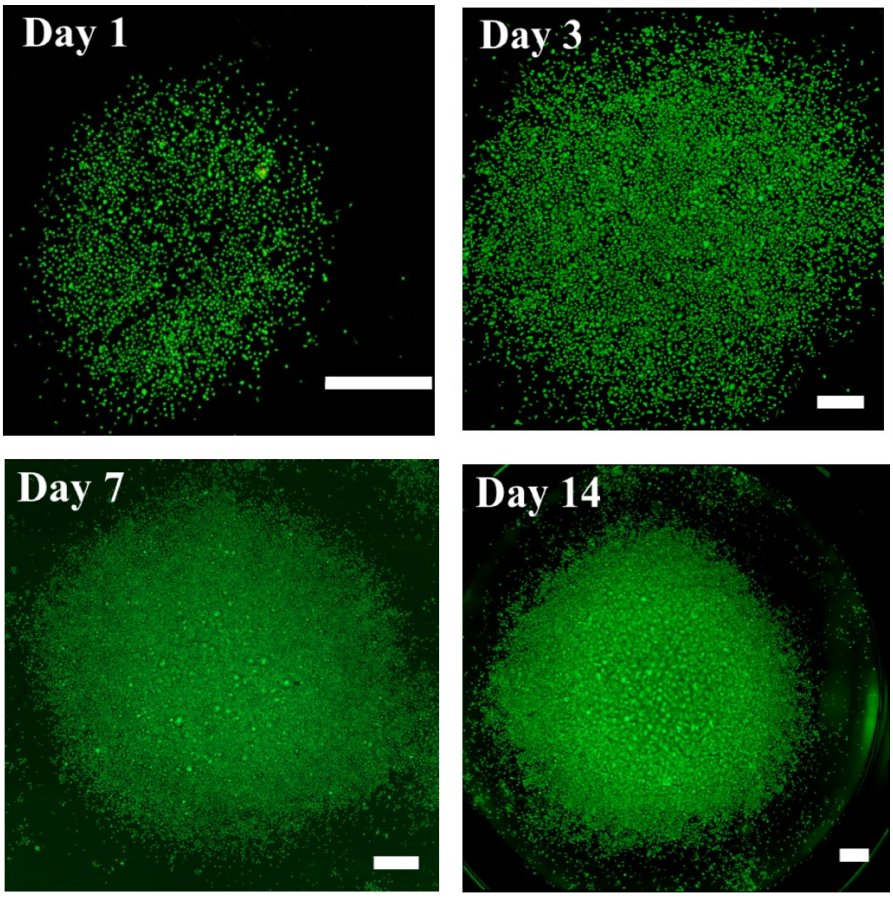

Figure 10 Representative images (2X) of the patterned colonies over time. C-AM (green)/PI (red) were used to stain the living and dead cells, respectively. Scale bars = 500 µm.

Cell Proliferation Analysis

As mentioned earlier, keratinocytes exhibit contact inhibition of proliferation. Based on this knowledge, I hypothesized that cells in the middle of the colony would undergo contact inhibition, while the cells near the edges of the colony would still proliferate and migrate to establish cell-cell contact. To investigate my hypothesis, I selected Ki-67, a cell proliferation marker present in the active stages of cell cycle, to examine the proliferation rates in both patterned and dispersedly-seeded conditions.

Cell growth was monitored for 14 days and the qualitative results of the cell proliferation assays are displayed in Figure 11. The representative images shown in Figure 11 were taken at the center of each well of the tissue culture plate. While it may appear that fewer proliferating cells (stained in green) are present in the initial days of the dispersedly-seeded condition, it is important to note that the cells are sparsely distributed across the well surface. Based on the qualitative results shown in Figure 11, the patterned condition showed a lower number of cells expressing the Ki-67 marker by day 14 compared to the dispersedly-seeded condition.

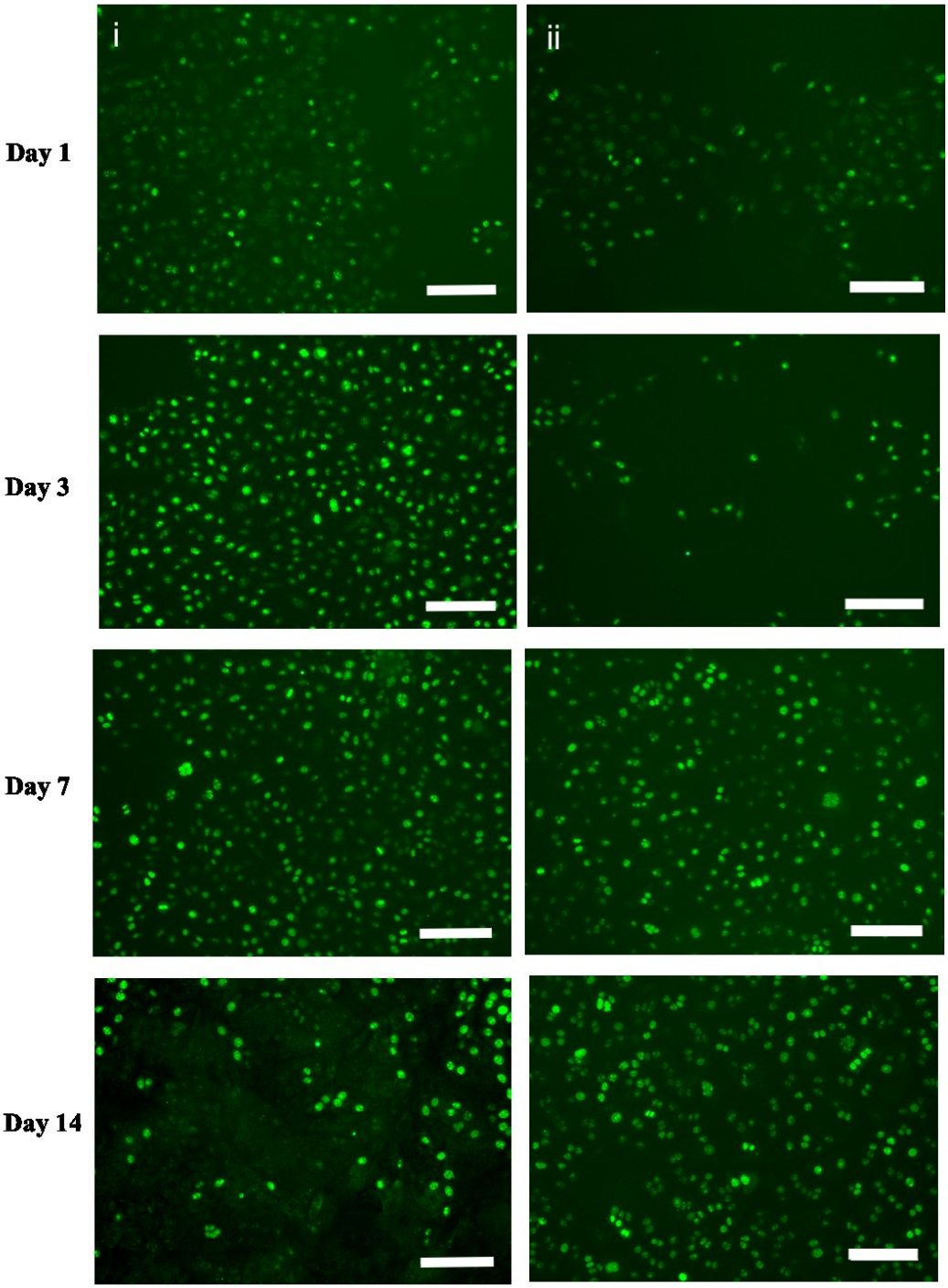

Figure 11 Cell proliferation assay.
Representative images (10X) of HEK001 cells expressing Ki-67 (green) in both patterned (i) and dispersedly-seeded (ii) cultures. Scale bars = 150 μm.

The results of the cell proliferating assay were further quantified using Fiji, as shown in Figure 12. The proliferation index (% total cells) represents the percentage of cells expressing the Ki-67 marker. Similar patterns of proliferation were observed for both patterned and dispersedly-seeded conditions on the initial day (Figure 12). However, the proliferation rates on days 7 and 14 revealed significant differences between the patterned and dispersedly-seeded conditions. Patterned conditions displayed lower proliferation rates as compared to the dispersedly-seeded conditions, suggesting that cells in the middle of the patterned colony are undergoing contact inhibition, while the cells at the periphery of the colony are proliferating and migrating to establish adherens junctions.

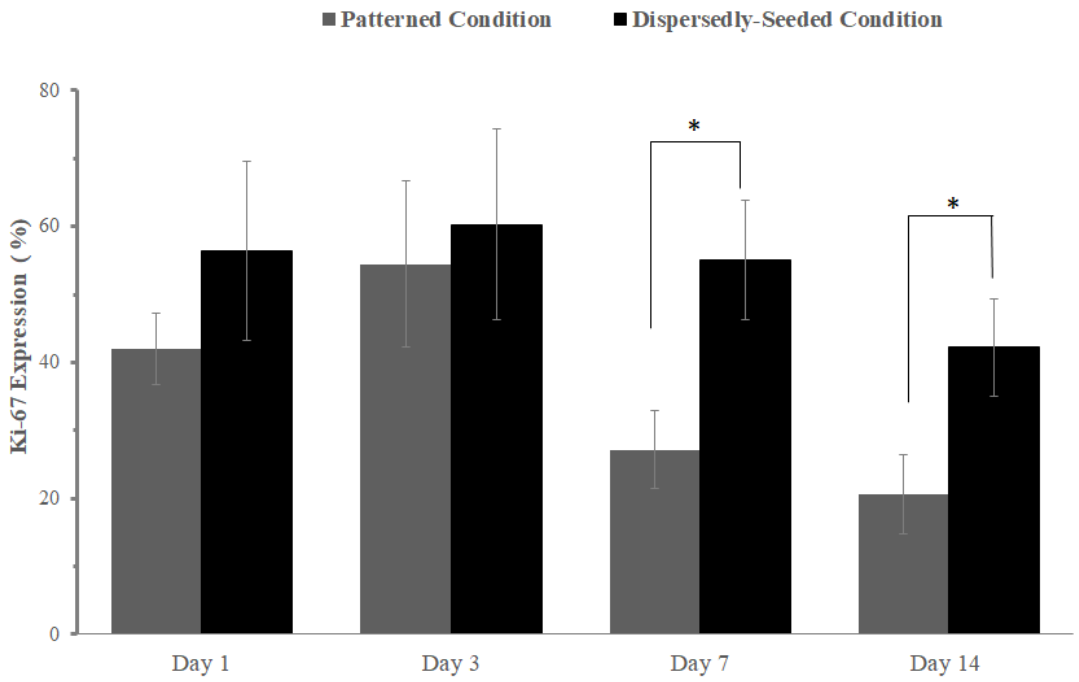

Figure 12 Quantification of Ki-67 expression in HEK001 cells.
The Y-axis represents Ki-67 expression in % of total cells and the X-axis represent the number of days. Values are the mean of three independent experiments and error bars represent the standard deviation of the mean values.

As mentioned earlier, contact inhibition is mediated by E-cadherin (*122*, *123*). Therefore, a lower percentage of proliferating cells and a greater percentage of differentiated cells are observed in the patterned cultures. To further confirm my hypothesis, expression of E-cadherin was examined in both conditions to measure the differences in barrier formation.

Assessment of formation of adherens junctions

The formation of adherens junction was evaluated by measuring the differences in E-cadherin expression in both conditions. E-cadherin is a Ca^{2+} (calcium (II) ion) dependent transmembrane protein that mediates cell-cell contact between the adjacent cells and forms intercellular junctions throughout the epidermis. Therefore, E-cadherin is commonly used as a marker for barrier formation in the epidermis. Cultures were monitored for 14 days. As shown in Figure 13, the patterned condition expressed higher E-cadherin levels than the dispersedly-seeded condition by day 14.

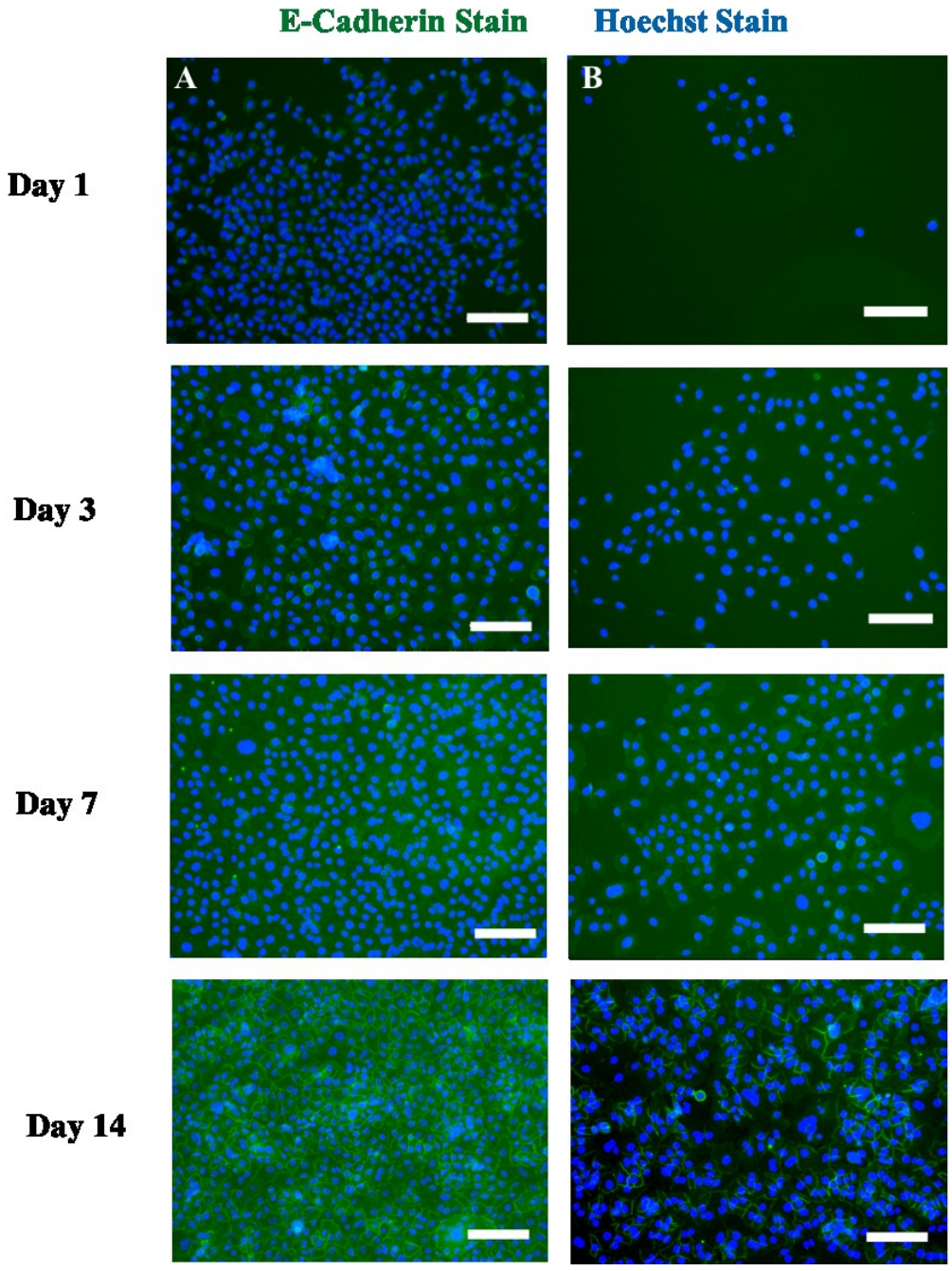

Figure 13 Formation of adherens junctions.
Representative images (10X) of Hoechst (blue) and formation of E-cadherin junctions (green) in both patterned (A) and dispersedly-seeded conditions (B). Scale bars = 150 μm.

While patterning the cells using the ATPS EBP approach had no impact on the formation of the adherens junctions on day 1, significant differences were revealed in E-cadherin expression between the conditions on days 3, 7, and 14 (Figure 14). This is to be expected as the cells in the patterned conditions readily establish cell-cell contact. However, the cells in the dispersedly-seeded condition are unable to contact each other, and therefore these cells continue to gradually proliferate and migrate. From these results, it can be inferred that the ATPS EBP approach is effective in delivering HEK001 cells and can be used to promote epidermal regeneration for future applications in skin tissue engineering.

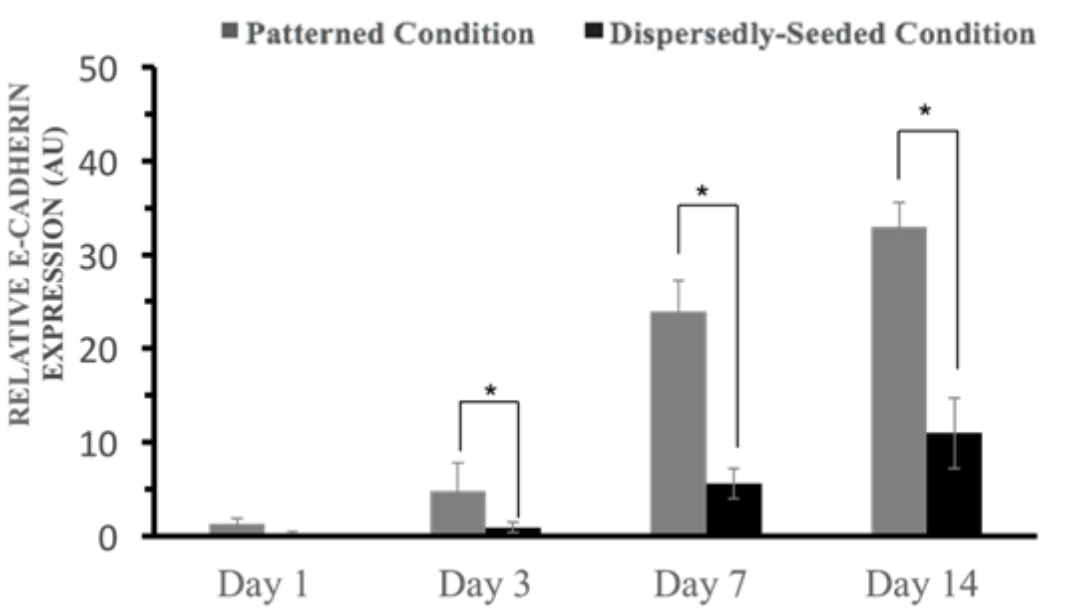

Figure 14 Quantification of relative expression of E-cadherin junctions in HEK001 cells.
Y-axis shows the relative expression of E-cadherin and number of days the cells are cultured are represented along the X-axis. AU denotes arbitrary units quantified from the thresholded image in Fiji. Error bars represents the standard deviation and relative expression values are means of three independent experiments.

In this section, I demonstrated the efficiency of my ATPS EBP approach by biopatterning HEK001 cells in colonies and comparing the barrier-forming abilities to the pre-existing cell seeding approaches Specifically, I compared cell viability, cell proliferation, and formation of adherens junctions. The cell viability assessment revealed that patterned conditions had high cell viability in the initial days, whereas ~50% cell death was observed in the dispersedly-seeded condition. Cell proliferation and formation of adherens junction were also analyzed. The results showed that cells in the patterned condition had a higher number of differentiated cells and a lower number of proliferating cells. Moreover, these conditions were able to develop an intact barrier by day 14, suggesting that ATPS EBP is useful in promoting keratinocyte growth and differentiation, which may be beneficial for wound healing and skin reconstruction applications.

A Potential Application of ATPS EBP Cell Delivery Approach

Cell-based therapies are advantageous as they result in rapid re-epithelization of the wound, increasing the wound closure rate along with a potential reduction in scar contracture. Conventional cell-based therapy uses autologous keratinocytes, which get transplanted onto a dermal substitute via cell spraying or seeding approaches. Although promising, these approaches result in poor cellular engraftment. Moreover, the limited availability of cells makes it challenging to fabricate a cell-dense construct like the epidermis in a clinically appropriate time frame. Similar observations were noted in my experiments when the cells were dispersedly-seeded onto tissue culture plates. The cells were not able to retain viability and more than 50% cell death was observed in these cultures on days 1 and 3. The sparse distribution of cells significantly delays the wound re-epithelialization process, as

the cells are unable to effectively communicate with each other via autocrine signaling. Despite the high proliferating rates in these cultures, fewer differentiated cells are found and therefore it takes several weeks for the cells to develop the epidermal barrier required for wound closure. However, my ATPS EBP technique allows patterning of cells in colonies, thereby accurately mimicking the natural growth environment of keratinocytes. Being in close proximity with one another allows the cells to readily establish cell-cell contact, which promotes growth and differentiation, as shown in Figures 8-14. These figures also highlight a key benefit of my technique in future clinical applications. The patterning achieved with ATPS EBP allows for concurrent proliferation and differentiation, resulting in barrier formation seven days earlier than the dispersedly-seeded condition. Given the same number of cells (5000 cells per colony), my technique could accelerate the process of re-epithelialization compared to the standard dispersedly-seeded condition. Additional studies will be required to determine the number of cells required for effective closure of wounds. Despite the benefits of ATPS EBP approach, one can conceivably argue that culture plate stiffness may confound or significantly influence the experimental results. Therefore, in the next section, I will be demonstrating a future clinical application of ATPS EBP technique by biopatterning cells directly onto a denuded dermal tissue to promote cell engraftment and epidermal regeneration.

3.3. Biopatterning of Keratinocytes on DermGEN™

3.3.1. Rationale

Various tissue engineering approaches have been used for restoring extensive skin loss. Attempts to treat such serious skin injuries involve the use of a skin substitute that helps

stabilize the wound matrix and supports tissue regeneration. One of the most common skin substitutes used in skin regeneration is the acellular dermal matrix. Acellular dermal matrices are decellularized tissues that retain the structure and function of the native dermal tissues. Although decellularized tissues are very effective in restoring the dermal wound bed, they are unable to support the epidermal reconstruction. For this reason, several cell-based therapies have been combined with acellular dermal matrix to repair full-thickness wounds. As highlighted in previous chapters, the standard cell-based therapies lack precision and are unable to re-epithelialize the wound surface, resulting in poor healing outcomes. Moreover, these cell-based therapies have also shown poor cellular engraftment. As a result, I wanted to assess the efficacy of the ATPS EBP approach in improving cell engraftment and epidermal regeneration. As demonstrated previously, my ATPS EBP was effective in promoting epidermal regeneration on tissue culture plates. By patterning cells using ATPS EBP, the printed cells were able to grow and differentiate rapidly to form an epidermal barrier. My technique gave much better results than the dispersedly-seeded condition, where cells proliferated more slowly and took seven days longer than the patterned conditions to form an epidermal barrier.

I saw that ATPS EBP could be a promising application for generating functional skin equivalents. I also wanted to demonstrate the clinical application of ATPS EBP as model for biopatterning directly on tissues. The previous study was conducted on a highly-uniform substrate (e.g., tissue culture plates) and there has yet to be any studies that examined the ability of ATPS EBP to maintain pattern fidelity on a topographically complicated substrate. To examine this, cells were patterned on an irregular decellularized

dermal tissue in discrete colonies using Blue-DEX and were assessed for pattern fidelity using a luminescence assay and Hoechst staining. Following this experiment, I hypothesized that patterning cells directly on a DermGEN™ tissue sample using my ATPS EBP technique will result in improved cell engraftment and stratum basale formation as compared to the dispersedly-seeded condition. Cell engraftment was characterized by luminescence production and stratum basale formation.

NOTE: A few section of this chapter has been adapted from an MRS Advances publication (please see Appendix A) (*101*).

3.3.2. Biopatterning of Keratinocytes on DermGEN™

In this aim, I wanted to investigate the ability of ATPS EBP approach to maintain pattern fidelity on an irregular, complex substrate such as a decellularized dermal matrix (DermGEN™) as a model for biopatterning directly on tissues. To test this, 5000 cells per colony were patterned using Blue-DEX droplets onto a 2cm x 2cm piece of DermGEN™ in a 4x4 microarray format (Figure 15). Blue-DEX was used to monitor the location of the printed colonies. A luminescence assay was used to examine the fidelity on day 3 of patterned cultures. The data revealed that ATPS EBP droplets were able to hold cells in their pattern on a topographically-complex substrate (Figure 15 B and C). Moreover, the cells were able to adhere to the DermGEN™, suggesting that ATPS EBP can preserve pattern fidelity on an irregular, complex substrate.

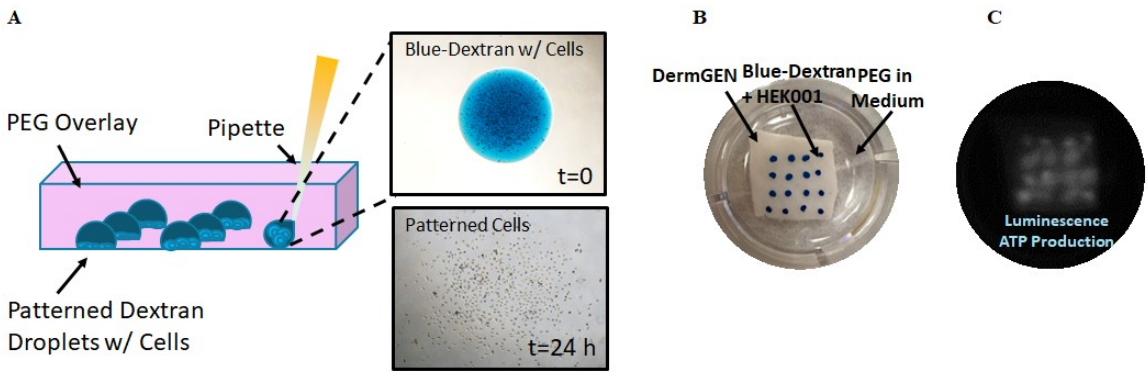

Figure 15 Biopatterning of cells on DermGEN™.
(A) Cartoon representation of cells patterned using Blue-DEX on DermGEN™. Images (4X) of cell printed on DermGEN™ were taken immediately post patterning (t=0) and 24 hours post patterning (t=24). (B) Representative image of 4x4 array of cells patterned on DermGEN™. ATPS EBP approach enabled cells to maintain pattern fidelity. (C) Representative luminescence images of cells engrafted on DermGEN™.

To further build upon the preliminary work, HEK001 cells were biopatterned in colonies on DermGEN™ constructs. As a control, the same number of cells were dispersedly-seeded onto DermGEN™ in each condition. Both conditions were monitored for cell engraftment and epidermal regeneration over 14 days (discussed in section 3.3.3 and 3.3.4.). The top-view images of Hoechst-labelled cells growing on DermGEN™ were also taken on day 14, as shown in Figure 16A. As can be seen in Figure 16B, the cells in the dispersedly-seeded condition were not uniformly distributed. This is most likely observed because of the irregularity and uneven surfaces of DermGEN™, which causes the cells to either localize at the edges of the matrix or fail to adhere to the DermGEN™ matrix, causing the cells to attach to the underlying tissue culture plates. In comparison, cells biopatterned on DermGEN™ construct using ATPS EBP were able to preserve their

fidelity and the cells were uniformly distributed across the denuded dermal surface, as shown in Figure 16B. These results indicate that the ATPS EBP technique is highly promising at confining cells and promoting cell attachment on irregular, complex substrates.

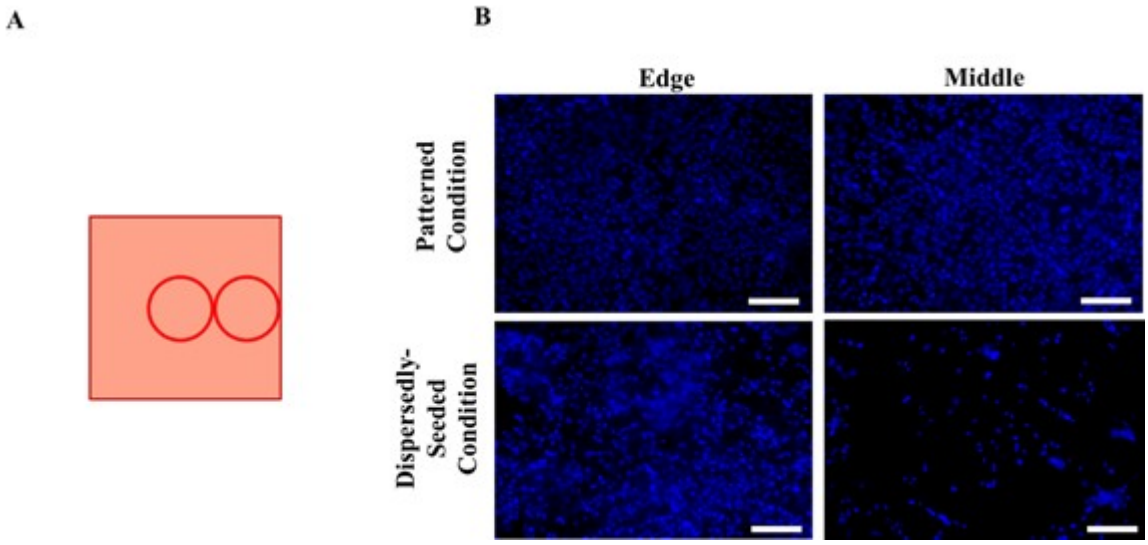

Figure 16 Representative images (10X) of Hoechst-labelled cells growing on DermGEN™.
(A) Cartoon representation of the top-view of DermGEN™. The cells on DermGEN™ were imaged at the middle and edge of the matrix. (B) Representative images (10X) of Hoechst-labelled cells (blue) in both patterned and dispersedly-seeded condition. Images were taken on day 14. Scale bars = 100 μm.

3.3.2. Cell Engraftment Analysis

As outlined previously, poor cell engraftment is one of the major challenges faced by the standard cell-based therapies. To address this issue, I further investigated the potential of ATPB EBP in promoting cell engraftment on DermGEN™. The efficacy of ATPS EBP in promoting cell engraftment was evaluated using the RealTime-Glo™ luminescence assay, which measures the reduction potential of cells and is directly correlated to the number of the living cells (refer to section 2.10.). Further, the luminescence assay enabled the imaging of cells growing on opaque substrates in real-time. As shown in Figure 17A, the cells in the patterned condition were able to retain their fidelity. It was also observed that the size of the printed colonies increased over time. The interspaced colonies eventually merged with each other to cover the entire surface of denuded dermal matrix by day 14 (Figure 17A). On the other hand, the cells in the dispersedly-seeded condition were unable to establish cell-cell contact, and as a result were unable to form a cell monolayer over the 14 days of the cultures (Figure 17A). The lack of luminescence in the dispersedly-seeded condition is mostly like observed because fewer cells engrafted on DermGEN™. Further quantification of the RealTime-Glo™ assay revealed that the patterned cells displayed higher luminescence production than the cells in the dispersedly-seeded condition (Figure 17B), suggesting that our ATPS EBP approach results in enhanced cell engraftment and growth of the engrafted cells on the dermal matrix.

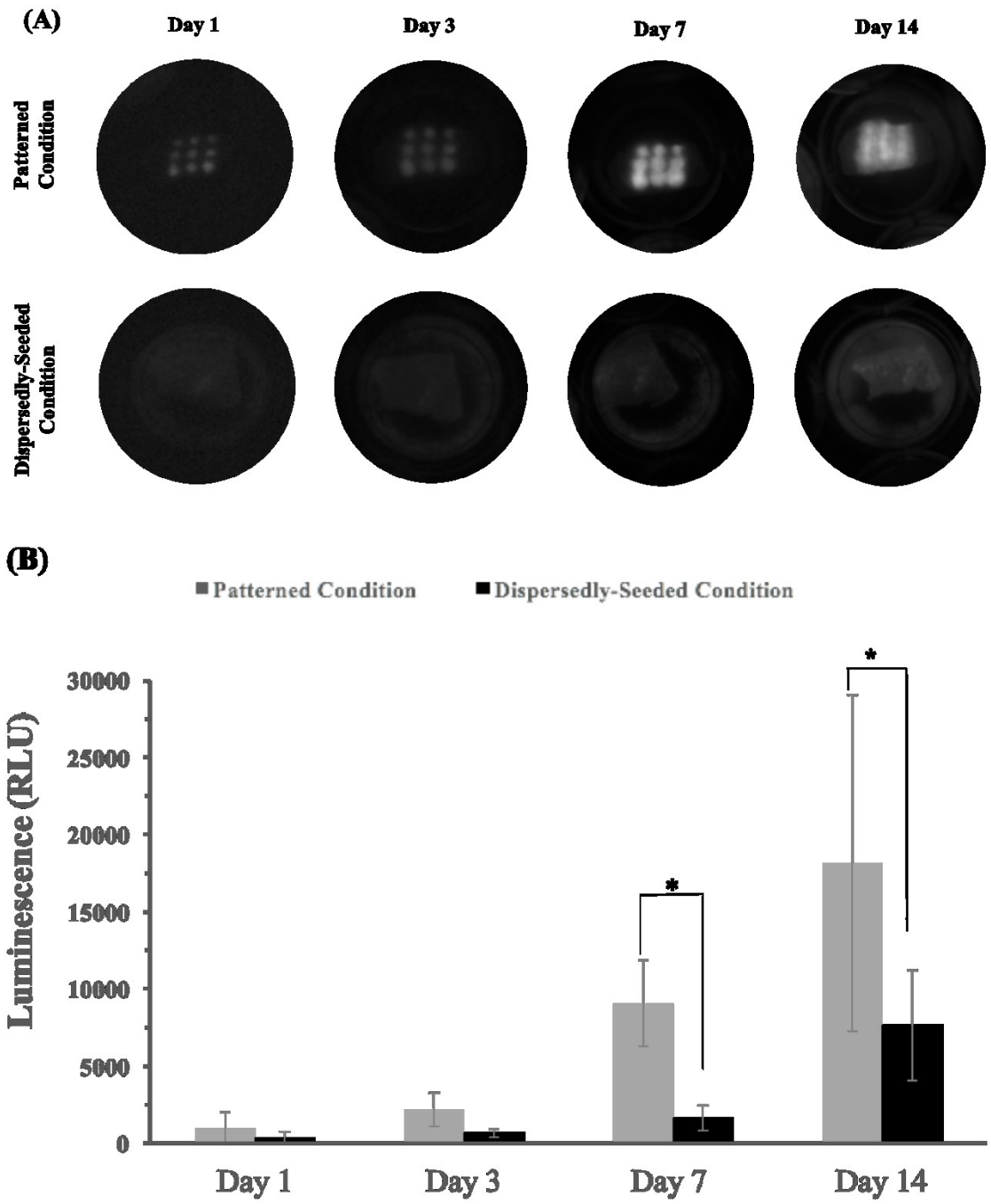

Figure 17 Cell engraftment on DermGEN™ using patterned and dispersedly-seeded cell delivery approaches.
(A) Representative luminescence images of HEK001 cells growing on DermGEN™ in both patterned and dispersedly-seeded conditions. These cultures were performed on treated tissue culture plates. (B) Quantification of luminescence in relative light units (RLU) for cells in both patterned and dispersedly-seeded conditions.

3.3.3. Cell Proliferation and Formation of Adherens Junctions on DermGEN™

The utility of the ATPS EBP approach was further investigated by monitoring cell engraftment and stratum basale formation on DermGEN™. The stratum basale is established by the basal cells, which proliferate and form a monolayer that further differentiate into suprabasal layers. To determine the efficiency of ATPS EBP in stratum basale formation, samples of acellular dermal matrix engrafted with patterned or dispersedly-seeded cells were processed and stained for H&E, Ki-67, and E-cadherin (refer to section 2.11.). H&E was used to stain the nucleus and cytoplasm, respectively (Figure 18). The H&E stain revealed that the cells in the patterned condition were able to form an intact stratum basale containing several layers of cells by day 14. It also appeared that a greater number of cells in the patterned condition were able to partially migrate into the decellularized matrix. On the other hand, the cells in the dispersedly-seeded condition were unable to cover the surface of the dermal matrix, and only a single cell layer was observed for these conditions (Figure 18).

Finally, we examined the ability of ATPS EBP to augment the growth and differentiation of keratinocytes on an acellular dermal matrix. Ki-67 and E-cadherin stainings were used to assess the tissue samples. The Ki-67 data revealed that the proliferation rates decreased after day 3 for the cells in patterned condition, while the proliferation rate for cells in the dispersedly-seeded condition did not decrease until after day 7 of the cultures (Figure 19). This is similar to what we observed when the cells were patterned on standard tissue culture plates. Next, E-cadherin was used to evaluate barrier formation capabilities of ATPS EBP

on dermal matrix (Figure 20). Similar results for E-cadherin expression to those noted in Figure 14 and 15 were observed for both condition. Figure 20 showed higher expression of E-cadherin for the cells patterned on days 7 and 14 using ATPS EBP approach than the control condition. The improved stratum basale formation for the patterned condition stems from the fact that the engrafted cells are presumably undergoing differentiation due to proximity of neighboring cells. Consequently, a higher number of differentiated and lower number of proliferating cells were found in the patterned condition. These result from biopatterning cells on dermal matrix further confirm the effectiveness of ATPS EBP in enhancing the growth and differentiation properties of keratinocytes in culture.

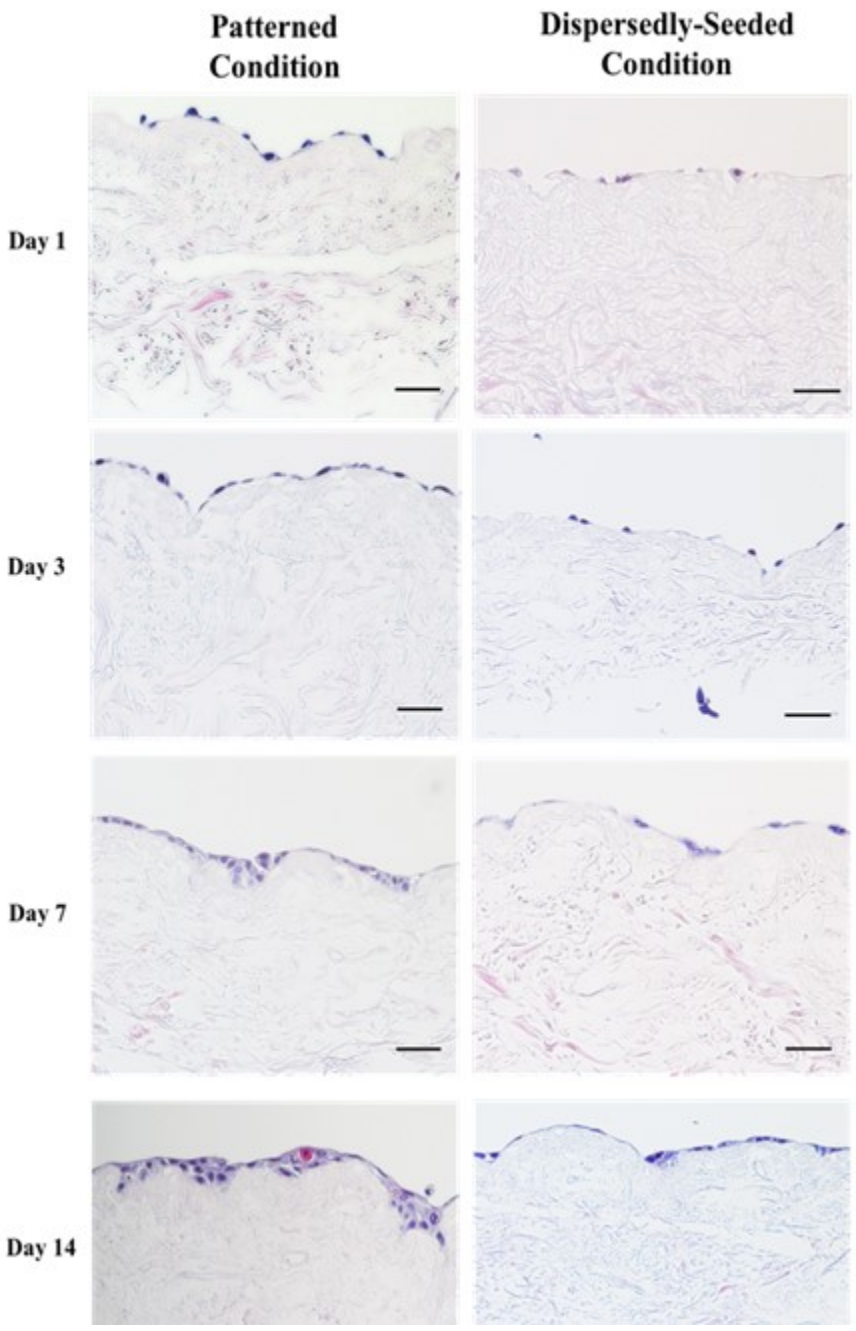

Figure 18 Representative images (20X) of Hematoxylin (purple) and Eosin (pink) (H&E) comparing cell engraftment and stratum basale formation in both patterned and dispersedly-seeded conditions.
Scale bars = 40 μm.

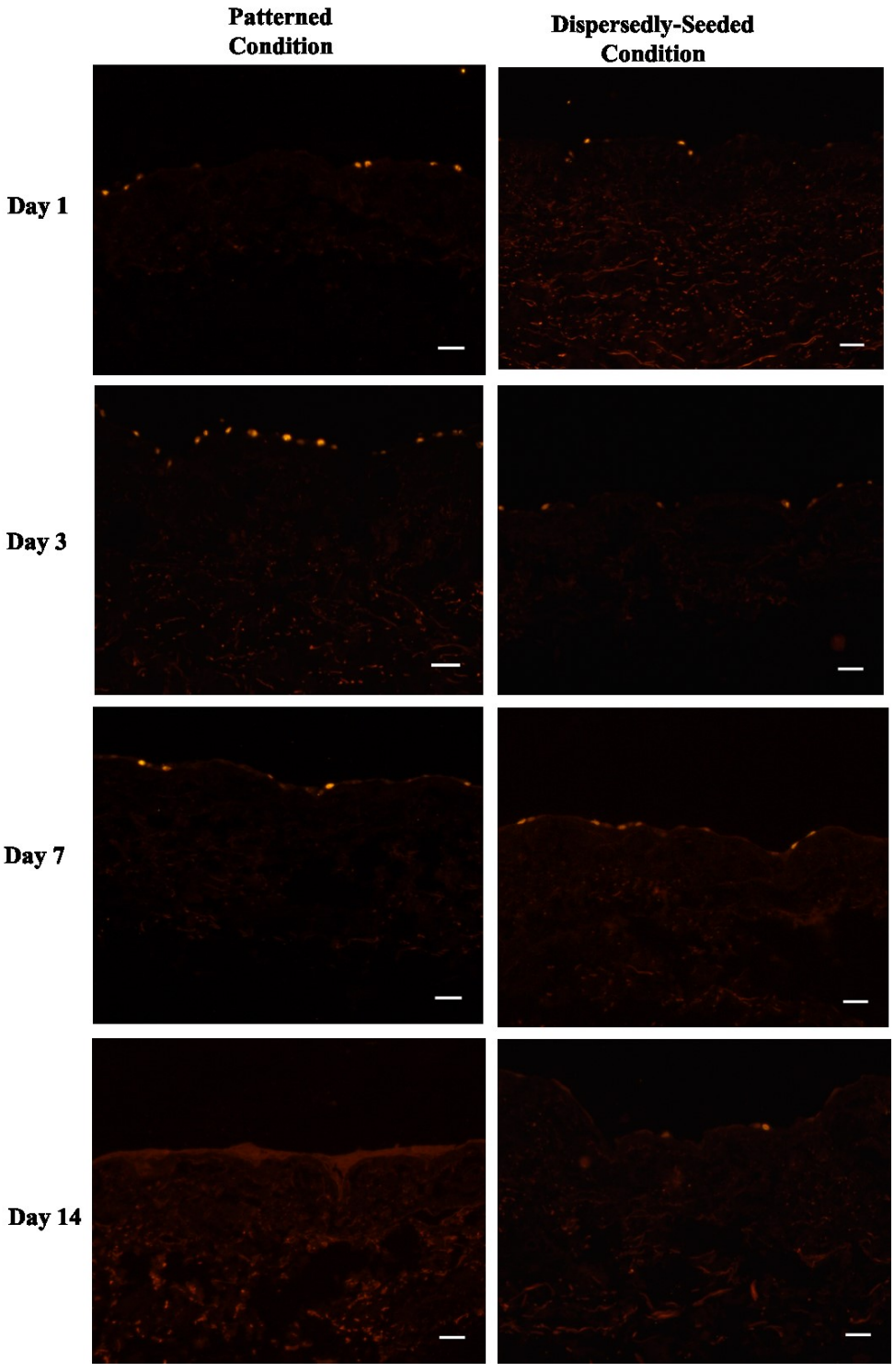

Figure 19 Representative images (10X) of Ki-67 (red) comparing stratum basale formation in both patterned and dispersedly-seeded conditions. Scale bars = 40 μm.

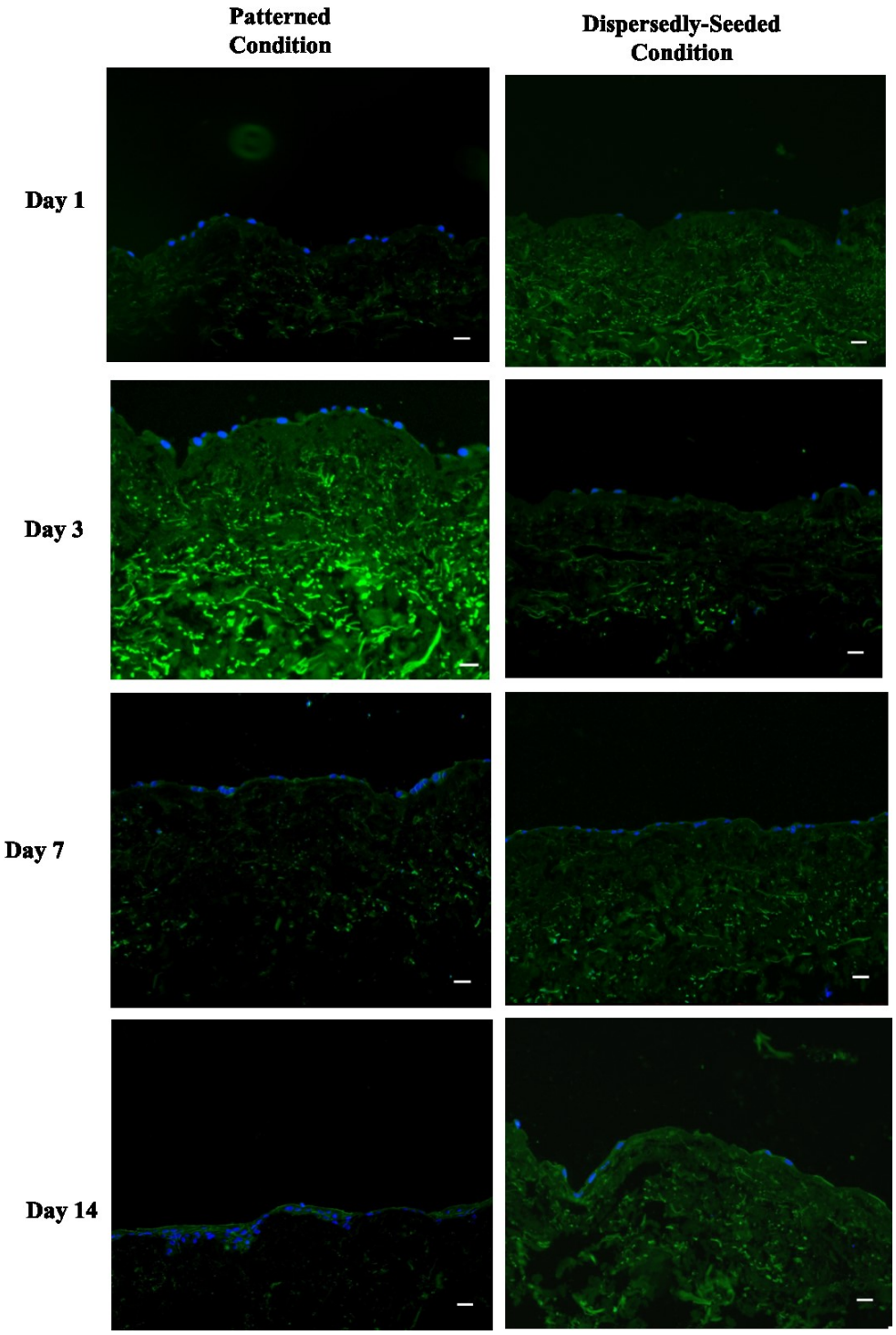

Figure 20 Representative images (10X) of E-cadherin (green) and Hoechst (blue) comparing stratum basale formation in both patterned and dispersedly-seeded conditions.
Scale bars = 40 μm.

Future work with ATPS EBP

Work demonstrated using ATPS EBP to deliver cells on acellular dermal matrix shows promising results. When the cells were patterned in colonies on the dermal matrix via ATPS EBP, the patterned colonies were able to retain their fidelity along with the enhanced engraftment of cells on the matrix. Although stratum basale formation was observed in the patterned cultures, the ability of ATPS EBP to complete differentiation of keratinocytes for epidermal construction still needs to be investigated. In this study, all the experiments were performed in submerged conditions (substrates immersed in culture medium) for 14 days, which may be too short of culture time to observe complete differentiation. Also, the submerged culture may not be sufficient to trigger the complete differentiation of these cells. As seen in the native skin tissue, epidermal cells are constantly exposed to air rather than the culture medium. Thus, the complete differentiation of epidermal cells from stratum basale to stratum corneum can be triggered by raising the cells from submerged environment to the air-liquid interface environments to produce more physiologically relevant tissues (*124*). Another factor that may affect the stratification process is the choice of cell type used for the study. Here, we demonstrated the application of ATPS EBP by patterning HEK001 cells. Since HEK001 cells are proliferating basal cell types, these cells lack the ability to form a fully stratified epidermal tissue. As an alternative, different cell lines such N/TERT keratinocytes has shown potential in generating epidermal models containing stratified layers (*125*). Therefore, future work would involve replicating the study using N/TERT keratinocytes to investigate if ATPS BEP can be used to form a fully stratified epidermis, which may be beneficial for wound healing and other skin reconstruction applications.

CHAPTER 4: CONCLUSION

Any skin injuries larger than 4 cm or more requires a graft to restore the structure and function of the damaged and/or diseased tissue. Although skin autografts still remain the gold standard for treating serious skin injuries, they have several drawbacks. To circumvent these limitations, several skin substitutes have been proposed for restoring extensive skin loss. While most of these substitutes are acellular in nature and have shown promises in restoring the dermal bed, these substitutes are unable to reconstruct the epidermis. Therefore, cell-based therapies (e.g., cell seeding and cell spraying) have been employed, but these approaches results in poor cellular engraftment. Moreover, the cell-based therapies lack precision and cannot accurately reflect the homotypic and heterotypic interactions needed for cell growth and differentiation. As a result, several biopatterning approaches have been used to precisely position biomolecules to analyze cell-cell interactions, proliferation, and differentiation. While all of these approaches are efficient, the versatility and cost-effectiveness of EBP makes it the most widely used approach. Despite the numerous benefits of EBP, one of the major limitations of EBP is the loss of pattern fidelity when printing on a wet substrate. Therefore, as a part of my thesis work, I developed a novel bio-ink for EBP that preserved both pattern fidelity and cell viability. I selected ATPSs comprised of phase-separating polymers such as PEG and DEX as a novel bioink for EBP. I used this ATPS EBP approach to address a several challenges in skin tissue engineering. I hypothesized that using ATPS EBP as a cell delivery approach would efficiently use limited numbers of cells and promote the self-assembly of a cell-dense construct. I also hypothesized that tight organization of cells in ATPS EBP would improve

growth and differentiation along with engraftment on an acellular dermal matrix. To achieve my goals, I first characterized the ATPSs-based ink to determine the optimal concentrations suitable for cell patterning. The combination of 5.0% PEG : 5.0% DEX resulted in stable and uniform pattern formation with excellent cell viability. These concentrations were then used to evaluate the effectiveness of my technique by comparing the growth and differentiation properties of cells in patterned conditions to the dispersedly-seeded approach. Conditions patterned using the ATPS EBP approach resulted in improved cell viability and formation of adherens junction, suggesting that ATPS EBP can be used to improve epidermal regeneration. A future clinical application of ATPS EBP was also demonstrated in this work. The cells were directly biopatterned on an acellular dermal matrix, DermGEN™, as a model for printing directly on tissue. The RealTime-Glo™ assay revealed that cells were able to maintain pattern fidelity on an uneven substrate. Moreover, the RealTime-Glo™ assay also showed higher number of viable cells in the patterned condition, suggesting that ATPS EBP improved cellular engraftment on the denuded dermal surface. Finally, cells patterned on acellular dermal matrices showed improved formation of adherens junction compared to the dispersedly-seeded condition, indicating that ATPS EBP is a promising technique that may have future applications in skin reconstruction and wound healing.

4.1. Statement of Contributions

1) I developed, optimized, and characterized a novel ATPSs-based ink for EBP that maintains pattern fidelity when biomolecules and cells are patterned on to a substrate immersed in cell culture medium. I also demonstrated that ATPS EBP retains cell viability and that the optimal polymer formulation is non-toxic to cells.
2) I applied ATPS EBP to efficiently biopattern human epidermal keratinocytes on standard tissue culture plates and decellularized dermal matrices. I demonstrated that ATPS EBP maintains pattern fidelity on a wet substrate.
3) I demonstrated that the 5.0% PEG and 5.0% DEX bio-ink produced excellent cell viability and is suitable for cell patterning.
4) I demonstrated the effectiveness of ATPS EBP by comparing cell growth and differentiation between patterned conditions and dispersedly-seeded conditions. My analysis revealed that the ATPS EBP cell delivery approach resulted in improved cell viability and formation of adherens junctions compared to the dispersedly-seeded approach.
5) I demonstrated proof-of-concept of a potential clinical application of ATPS EBP by biopatterning cells onto DermGEN™. My analysis revealed that ATPS EBP maintain pattern fidelity on the uneven surface of DermGEN™.
6) I demonstrated improved cellular engraftment on DermGEN™. My analysis revealed the formation of an epidermal barrier on both tissue culture plates and DermGEN™, suggesting the potential use of ATPS EBP in generating functional skin equivalents.

4.2. Future Work

1) The regional variation in cell viability, proliferation and E-cadherin expression across biopatterned colonies and dispersedly-seeded conditions will require further assessment. This work will be competed very soon and will be published in forthcoming manuscript.
2) As mentioned previously, cells have been patterned in a range of configurations *in vitro.* In this work, cells were patterned on DermGEN™ in a 3x3 micorarray format. However, it would be interesting to pattern cells in range of different configurations and examine the differences in cell growth and differentiation based on geometric patterns.
3) The experiments in this work were performed using simple handheld micropipettors. However, combining ATPS EBP approach with sophisticated liquid-handling robots, ADE, or microfluidic devices will allow generation of complex patterns in a high-throughput manner.
4) All experiments for biopatterning on DermGEN™ were performed in submerged cultures. Future work would involve exploring different environmental conditions, such as air-liquid interface, for stratification of the epidermis.
5) In this work, HEK001 was used to examine the efficiency of ATPS EBP approach. However, this cell line only expresses keratin 14 and therefore HEK001 cell lines are unable to form a fully stratified epithelium. Smits et al. demonstrated immortalized N-TERT keratinocytes as an alternative cell source that are capable of generating human epidermal models (*125*). Future work would involve using

ATPS EBP to biopattern N-TERT or primary keratinocytes from donor tissue to generate a fully functional skin equivalent.

6) Skin is a highly complex structure with multiple cell types along with various skin appendages. This work focuses on only one of the major cell types, keratinocytes. Future work should involve patterning of co-cultures to accurately mimic the cellular composition of skin tissue.
7) Characterization of distance between the droplets along with the droplet sizes will allow us to determine the appropriate spacing needed for rapid wound re-epithelialization.

BIBLIOGRAPHY

1. R. A. F. Clark, K. Ghosh, M. G. Tonnesen, Tissue engineering for cutaneous wounds. *J. Invest. Dermatol.* **127**, 1018–1030 (2007).
2. M. Balasubramani, T. R. Kumar, M. Babu, Skin substitutes: a review. *Burns*. **27**, 534–544 (2018).
3. M. Pasparakis, I. Haase, H. O. Nestle, Mechanism regulating skin immunity and inflammation. *Nat. Rev. Immunol.* 1**4**, 289-301 (2014).
4. R. R. Seeley, S. Trent D, P. Tate, The integumentary system in *Anatomy and Physiology*. (2003), 144–164.
5. E. Mclafferty, C. Hendry, F. Alistair, The integumentary system: anatomy, physiology and function of skin. *Nurs. Stand.* **27**, 35–43 (2012).
6. D. J. Wong, H. Y. Chang, Skin Tissue Engineering in *Stembook.* (2009), 1–8.
7. P. A. J. Kolarsick, M. A. Kolarsick, C. Goodwin, Anatomy and physiology of the skin in *Skin Cancer*. (2006), 1-11.
8. P. Bensouilah, J., & Buck, Aromatherapy in Treatment and Care of Common Skin Conditions in *Aromadermatology*. (2006), 1–11.
9. H. Sun, T., Green, Differentiation of the epidermal keratinocytes in cell culture: formation of the cornified envelope. *Cell*. **9**, 511-521 (1976).
10. J. A. Segre, Epidermal barrier formation and recovery in skin disorders. *J. Clin. Invest.* **116**, 1150–1158 (2006).
11. P. Cartlidge, The Epidermal Barrier. *Semin. Neonatol*. **5**, 273–280 (2000).
12. A. Gord, W. R. Holmes, X. Dai, Q. Nie, Computational modelling of epidermal stratification highlights the importance of asymmetric cell division for predictable and robust layer formation. *J. R. Soc. Interface*. **11**, 1-13 (2014).
13. C. Blanpain, E. Fuchs, Epidermal homeostasis: a balancing act of stem cells in the skin. *Nat. Rev. Mol. Cell Biol.* **10**, 207–217 (2009).
14. M. I. Koster, Making an epidermis. *Ann. N. Y. Acad. Sci*. **1170**, 7–10 (2009).
15. G. Schmitz, G. Müller, Structure and function of lamellar bodies, lipid-protein complexes involved in storage and secretion of cellular lipids. *J. Lipid Res*. **32**, 1539–1570 (1991).
16. K. Fukuyama, W. L. Epstein, Keratohyalin in *Biology of the Integument*. (1986), 739–751.
17. T. C. Wikramanayake, O. Stojadinovic, M. Tomic-Canic, Epidermal differentiation in barrier maintenance and wound healing. *Adv. Wound Care*. **3**, 272–280 (2014).

18. L. Eckhart, S. Lippens, E. Tschachler, W. Declercq, Cell death by cornification. *Biochim. Biophys. Acta - Mol. Cell Res*. **1833,** 3471–3480 (2013).

19. P. D. Yurchenco, B. L. Patton, Developmental and pathogenic mechanisms of basement membrane assembly. *Curr. Pharm. Des*. **15**, 1277–1294 (2009).

20. J. R. McMillan, M. Akiyama, H. Shimizu, Epidermal basement membrane zone components: ultrastructural distribution and molecular interactions. *J. Dermatol. Sci.* **31**, 169–177 (2003).

21. D. Breitkreutz, N. Mirancea, R. Nischt, Basement membranes in skin: unique matrix structures with diverse functions. *Histochem. Cell Biol*. **132**, 1–10 (2009).

22. M. S. Roberts, The structure and function of skin in *Dermatological and Transdermal Formulations*. (2002), 1-31.

23. A. D. Metcalfe, M. W. J. Ferguson, Tissue engineering of replacement skin: the crossroads of biomaterials, wound healing, embryonic development, stem cells and regeneration, **4**, 413–437 (2007).

24. S. Vijayavenkataraman, W. F. Lu, J. Y. Fuh, 3D bioprinting of skin: a state-of-the-art review on modelling, materials, and processes. *Biofabrication*. **8**, 1–31 (2016).

25. S. Das, A. B. Baker, Biomaterials and nanotherapeutics for enhancing skin. *Wound Healing*. **4**, 1–20 (2016).

26. G.S. Lazarus, D. M. Cooper, D. R. Knighton, D. J. Margolis, R. E. Pecoraro, G. Rodeheaver, M.C. Robson, Definitions and guidelines for assessment of wounds and evaluation of healing. *Wound Repair Regen*. **2**, 165–170 (2002).

27. T. Velnar, T. Bailey, V. Smrkolj, The wound healing process: an overview of the cellular and molecular mechanisms. *J. Int. Med. Res*. **37**, 1528–1542 (2009).

28. R. V Shevchenko, S. L. James, S. E. James, A review of tissue-engineered skin bioconstructs available for skin reconstruction. *J. R. Soc. Interface*. **7**, 229–258 (2010).

29. S. Macneil, Progress and opportunities for tissue-engineered skin. *Nature*. **445**, 874-880 (2007).

30. D. N. Herndon, R. E. Barrow, R. L. Rutan, T. C. Rutan, M. H. Desai, S. Abston, A comparison of conservative versus early excision. Therapies in severely burned patients. *Ann. Surg*. **209**, 547–553 (1989).

31. A. J. Singer, R. A. F. Clark, Cutaneous wound healing. *N. Engl. J. Med*. **341**, 738–746 (1999).

32. G. C. Gurtner, S. Werner, Y. Barrandon, M. T. Longaker, Wound repair and regeneration. *Nature*. **453**, 314- 321 (2008).

33. A. Ikramuddin, Biology of wound healing. *Periodontol*. **22**, 44–50 (2003).

34. K. A. Bielefeld, S. Amini-Nik, B. A. Alman, Cutaneous wound healing: recruiting developmental pathways for regeneration. *Cell. Mol. Life Sci*. **70**, 2059–2081 (2013).

35. J. A. Schilling, Wound healing. *Physiol. Rev*. **48**, 374–423 (1968).

36. H. Sinno, S. Prakash, Complements and the wound healing cascade: an updated review. *Plast. Surg. Int*. **2013**, 146764–146770 (2013).

37. P. Martin, Wound healing – aiming for perfect skin regeneration. *Science*. **276**, 75-81 (1997).

38. A. C. de O. Gonzalez, T. F. Costa, Z. de A. Andrade, A. R. A. P. Medrado, Wound healing - a literature review. *An. Bras. Dermatol*. **91**, 614–620 (2016).

39. T. H. Adair, J. P. Montani, Overview of angiogenesis in *Angiogenesis*. (2010).

40. M. Takeo, W. Lee, M. Ito, Wound healing and skin regeneration. *Cold Spring Harb. Perspect. Med.* **5**, a0232367 (2015).

41. J. A. Sherratt, J. D. Murray, Models of epidermal wound healing. *Proc. R. Soc. London. Ser. B Biol. Sci*. **241**, 29-36 (1990).

42. M. Tscharntke, R. Pofahl, A. Chrostek-Grashoff, N. Smyth, C. Niessen, C. Niemann, B. Hartwig, V. Herzog, H. W. Klein, T. Krieg, C. Brakebusch, I. Haase, Impaired epidermal wound healing in vivo upon inhibition or deletion of Rac 1. *J. Cell Sci*. **120**, 1480-1490 (2007).

43. I. Pastar, O. Stojadinovic, N. C. Yin, H. Ramirez, A. G. Nusbaum, A. Sawaya, S. B. Patel, L. Khalid, R. R. Isseroff, M. Tomic-Canic, Epithelialization in wound healing: a comprehensive review. *Adv. Wound Care*. **3**, 445–464 (2014).

44. J. A. Sherratt, J. C. Dallon, Theoretical models of wound healing: past successes and future challenges. *C. R. Biol*. **325**, 557–564 (2002).

45. D. Ratner, Skin Grafting. From Here to There. *Dermatol. Clin.***16**, 75–90 (1998).

46. A. Andreassi, R. Bilenchi, M. Biagioli, C. D. Aniello, Classification and pathophysiology of skin grafts. *Clin. Dermatol.***23**, 332–337 (2005).

47. H. Green, O. Kehinde, J. Thomas, Growth of cultured human epidermal cells into multiple epithelia suitable for grafting, *Proc. Natl. Acda. Sci. USA.* **76**, 5665–5668 (1979).

48. Genzyme, Epicel (cultured epidermal autografts). *U.S. FDA.* 1–11 (2015).

49. M. N. Nicholas, J. Yeung, Current status and future of skin substitutes for chronic wound healing. *J. Cutan. Med. Surg.* **21,** 23-30 (2017).

50. G. Naughton, J. Mansbridge, G. Gentzkow, A metabolically active human dermal replacement for the treatment of diabetic foot ulcers. *Artif. Organs.* **21**, 1203–1210 (1997).

51. W. Marston, J. Hanft, P. Norwood, R. Pollak, The efficacy and safety of Dermagraft in improving the healing of chronic diabetic foot ulcers. *Diabetes Care*. **26**, 1701–1705 (2003).

52. G. D. Gentzkow, S. D. Iwasaki, K. S. Hershon, M. Mengel, J. J. Prendergast, J. J. Ricotta, D. P. Steed, S. Lipkin, Use of dermagraft, a cultured human dermis, to treat diabetic foot ulcers. *Diabetes Care*. **19**, 350-354 (1996).

53. A. S. Landsman, J. Cook, E. Cook, A. R. Landsman, P. Garrett, J. Yoon, A. Kirkwood, E. Desman, A retrospective clinical study of 188 consecutive patients to examine the effectiveness of a biologically active cryopreserved human skin allograft (TheraSkin ®) on the treatment of diabetic foot ulcers and venous leg ulcers. *Foot Ankle Spec*. **4**, 29–41 (2010).

54. S. Misra, P. Heldin, V. C. Hascall, N. K. Karamanos, S. S. Skandalis, R. R. Markwald, S. Ghatak, Hyaluronan-CD44 interactions as potential targets for cancer therapy. *FEBS J*. **278**, 1429–1443 (2011).

55. Shire Executes Agreement to Divest Dermagraft. Shire Press Release (2014).

56. R. S. Kirsner, G. Bohn, V. R. Driver, J. L. Mills, L. B. Nanney, M. L. Williams, S. C. Wu, Human acellular dermal wound matrix: evidence and experience. *Int. Wound J*. **12**, 646–654 (2015).

57. J. A. Faleris, R. M. C. Hernandez, D. Wetzel, R. Dodds, D. C. Greenspan, In-vivo and in-vitro histological evaluation of two commercially available acellular dermal matrices. *Hernia*. **15**, 147–156 (2011).

58. T. W. Gilbert, J. M. Freund, S. F. Badylak, Quantification of DNA in biologic scaffold materials. *J. Surg. Res*. **152**, 135–139 (2009).

59. P. F. Gratzer, K. Conlan, A. Murphy, A new decellularized dermal matrix: superior properties and in-vivo performance when compared with the leading commercial product. *Front. Bioeng. Biotechnol.* (2016).

60. H.-J. You, S.-K. Han, Cell therapy for wound healing. *J. Korean Med. Sci*. **29**, 311–319 (2014).

61. G. Gallico, N. E. O'Connor, C. C. Compton, J. P. Remensnyder, O. Kehinder, H. Green, Cultured epithelial autografts for giant congenital nevi. *Plast. Reconstr. Surg*. **84**, 1–9 (1989).

62. G. G. Gallico, N. E. O'Connor, C. C. Compton, O. Kehinde, H. Green, Permanent coverage of large burn wounds with autologous cultured human epithelium. *N. Engl. J. Med*. **311**, 448–451 (1984).

63. A. W. Chua, Y. C. Khoo, B. K. Tan, C. L. Foo, S. J. Chong, Skin tissue engineering advances in severe burns: review and therapeutic applications. *Burn. Trauma*. **4**, 1–14 (2016).

64. R. S. Kirsner, W. A. Marston, R. J. Snyder, T. D. Lee, D. I. Cargill, H. B. Slade, Spray-applied cell therapy with human allogeneic fibroblasts and keratinocytes for the treatment of chronic venous leg ulcers: a phase 2,

multicentre, double-blind, randomised, placebo-controlled trial. *Lancet*. **380**, 977–985 (2012).

65. W. Peng, D. Unutmaz, I. T. Ozbolat, Bioprinting towards physiologically relevant tissue models for pharmaceutics. *Trends Biotechnol*. **34**, 722–732 (2016).

66. R. Klebe, Cytoscribing: a method for micropositioning cells and the construction of two-and three- dimensional synthetic tissue. *Exp. Cell Res*. **179**, 362–373 (1988).

67. I. T. Ozbolat, W. Peng, V. Ozbolat, Application areas of 3D bioprinting. *Drug Discov. Today.* **21**, 1257–1271 (2016).

68. J. Li, M. Chen, X. Fan, H. Zhou, Recent advances in bioprinting techniques: approaches, applications and future prospects. *J. Transl. Med*. **14**, 271 (2016).

69. S. Jana, A. Lerman, Bioprinting a cardiac valve. *Biotechnol. Adv*. **33**, 1503–1521 (2015).

70. A. Bakhshinejad, R. M. D. Souza, A brief comparison between available Bio-printing Methods, 1–4.

71. B. Guillotin, A. Souquet, S. Catros, M. Duocastella, B. Pippenger, S. Bellance, R. Bareille, M. Remy, L. Bordenace, J. Amedee, F. Guillemot, Laser assisted bioprinting of engineered tissue with high cell density and microscale organization. *Biomaterials*. **31**, 7250–7256 (2010).

72. X. Zhang, Y. Zhang, Tissue engineering applications of three-dimensional bioprinting. *Cell Biochem. Biophys*. **72**, 777–782 (2015).

73. S. Michael, H. Sorg, C. T. Peck, L. Koch, A. Deiwick, B. Chichkov, P. M. Vogt, K. Reimers, Tissue engineered skin substitutes created by laser- assisted bioprinting form skin-like structures in the dorsal skin fold chamber in mice. *PloS one*. **8**, e57741 (2013).

74. I. T. Ozbolat, M. Hospodiuk, Biomaterials current advances and future perspectives in extrusion-based bioprinting. *Biomaterials*. **76**, 321–343 (2016).

75. K. Jakab, C. Norotte, B. Damon, F. Marga, A. Neagu, C. L. Besch-Williford, A. Kachurin, K. H. Church, H. Park, V. Mironov, R. Markawald, G. Vunjak-Novakovic, G. Forgacs, Tissue engineering by self-assembly of cells printed into topologically defined structures. *Tissue Eng. Part A*. **14**, 413–421 (2008).

76. A. Skardal, J. Zhang, G. D. Prestwich, Bioprinting vessel-like constructs using hyaluronan hydrogels crosslinked with tetrahedral polyethylene glycol tetracrylates. *Biomaterials*. **31**, 6173–6181 (2010).

77. G. Kim, S. Ahn, Y. Kim, Y. Cho, W. Chun, Coaxial structured collagen–alginate scaffolds: fabrication, physical properties, and biomedical application for skin tissue regeneration. *J. Mater. Chem*. **21**, 6165–6172 (2011).

78. V. Lee, G. Singh, J. P. Trasatti, C. Bjornsson, X. Xu, T. N. Tran, S. S. Yoo, G. Dai, P. Karande, Design and fabrication of human skin by three-dimensional bioprinting. *Tissue Eng. Part C. Methods*. **20**, 473–484 (2014).

79. P. Calvert, Printing Cells. *Science*. **318**, 208-209 (2007).

80. J. A. Benavides, J. Rito-Palomares, M. Asenjo, in *Comprehensive Biotechnology.* (2011), 697–713.

81. P. A. K. Albertsson in *Partition of cell particles and macromolecules: separation and purification of biomolecules, cell organelles, Membranes, and cells in aqueous polymer two-phase systems and their use in biochemical analysis and biotechnology* (1986).

82. A. M. Grilo, M.R. Aires-Barros, A. M. Azevedo, Partitioning in aqueous two-phase systems: fundamentals, applications and trends. *Sep. Purif. Rev*. **45**, 68–80 (2014).

83. M. Iqbal, Y. Tao, S. Xie, Y. Zhu, D. Chen, X. Wang, L. Huang, D. Peng, A. Sattar, M. A. B. Shabbir, H. I. Hussain, S. Ahmed, Z. Yuan, Aqueous two-phase system (ATPS): an overview and advances in its applications. *Biol. Proced. Online*. **18**, 18 (2016).

84. J. Esquena, Water-in-water (W/W) emulsions. *Curr. Opin. Colloid Interface Sci*. **25**, 109–119 (2016).

85. P.-Å. Albertsson, in *Partitioning in aqueous two-phase system, H. Walter, Ed*. (1985), 1–10.

86. P.-Å. Albertsson, in *Partition of cell particles and macromolecules; distribution and fractionation of cells, mitochondria, chloroplasts, viruses, proteins, nucleic acids, and antigen-antibody complexes in aqueous polymer two-phase systems*. (1971).

87. S. Hardt, T. Hahn, Microfluidics with aqueous two-phase systems. *Lab. Chip*. **12**, 434–42 (2012).

88. R. Hatti-Kaul, in *Aqueous two-phase systems: methods and protocols, methods in biotechnology*. (2000), 1–10.

89. D. F. Silva, A. M. Azevedo, P. Fernandes, V. Chu, J. P. Conde, M. R. Aires-Barros, Design of a microfluidic platform for monoclonal antibody extraction using an aqueous two-phase system. *J. Chromatogr. A*. **1249**, 1–7 (2012).

90. T. Kojima, S. Takayama, Microscale determination of aqueous two-phase system binodals by droplet dehydration in oil. *Anal. Chem*. **85**, 5213–5218 (2013).

91. D. F. Silva, A. M. Azevedo, P. Fernandes, V. Chu, J. P. Conde, M. R. Aires-Barros, Determination of aqueous two-phase system binodal curves using a microfluidic device. *J. Chromatogr. A*. **1370**, 115–120 (2014).

92. M. Ruthven, K. R. Ko, R. Agarwal, J. P. Frampton, S. Takayama, Microscopic evaluation of aqueous two-phase system emulsion characteristics

enables rapid determination of critical polymer concentrations for solution micropatterning. *Analyst*. **142**, 1938–1945 (2017).

93. R. D'souza, A.A. Shegokar, Polyethylene glycol (PEG): a versatile polymer for pharmaceutical applications. Expert Opin. Drug Deliv. 13, 1257–1275 (2016).

94. A. Banerjee, R. Bandopadhyay, Use of dextran nanoparticle: A paradigm shift in bacterial exopolysaccharide based biomedical applications. *Int. J. Biol. Macromol*. **87**, 295–301 (2016).

95. H. Tavana, A. Jovic, B. Mosadegh, Q. Y. Lee, X. Liu, K. E. Luker, G. D. Luker, S. J. Weiss, S. Takayama, Nanoliter liquid patterning in aqueous environments for spatially-defined reagent delivery to mammalian cells. *Nat. Mater*. **8**, 736–741 (2009).

96. H. Tavana, B. Mosadegh, P. Zamankhan, J. B. Grotberg, S. Takayama, Microprinted feeder cells guide embryonic stem cell fate. *Biotechnol. Bioeng*. **108**, 2509–2516 (2011).

97. E. Atefi, R. Joshi, J. A. Mann, H. Tavana, Interfacial tension effect on cell partition in aqueous two-phase systems. ACS Appl. Mater. Interfaces. 7, 21305–21314 (2015).

98. H. Tavana, K. Kaylan, T. Bersano-Begey, K. E. Luker, G. D. Luker, S. Takayama, Rehydration of Polymeric aqueous biphasic system rehydration facilitates high throughput cell exclusion patterning for cell migration studies. *Adv. Funct. Mater*. **21**, 2920–2926 (2011).

99. J. P. Frampton, J. B. White, A. T. Abraham, S. Takayama, Cell co-culture patterning using aqueous two-phase systems. *J. Vis. Exp*. **73**, 16–20 (2013).

100. E. Atefi, D. Eyffe, K. B. Kaylan, H. Tavana, Characterization of aqueous two-phase systems from volume and density measurements. *J. Chem. Eng. Data*. **61**, 1531–1539 (2016).

101. R. Agarwal, K. R. Ko, P. F. Gratzer, J. P. Frampton, Biopatterning of keratinocytes in aqueous two-phase systems as a potential tool for skin tissue engineering. *MRS Adv*. **2**, 2443-2449 (2017).

102. S. A. Weston, C. R. Parish, New fluorescent dyes for lymphocyte migration studies: Analysis by flow cytometry and fluorescence microscopy. *J. Immunol. Methods*. **133**, 87–97 (1990).

103. T. Suzuki, K. Fujikura, T. Higashiyama, K. Takata, DNA staining for fluorescence and laser confocal microscopy. *J. Histochem. Cytochem*. **45**, 49–53 (1997).

104. G. Johannes, S. Ulrich, L. Hilmar, S. Harald, Production of a mouse monoclonal antibody reactive with a human nuclear antigen associated with cell proliferation. *Int. J. Cancer*. **31**, 13–20 (2006).

105. A. Hartsock, W. J. Nelson, Adherens and tight junctions: structure, function and connections to the actin cytoskeleton. *Biochim. Biophys. Acta*. **1778**, 660–669 (2008).

106. R. Davidson, K. A. O'Malley, T. B. Wheeler, Polyethylene glycol-induced mammalian cell hybridization: effect of polyethylene glycol molecular weight and concentration. *Somat. Cell Genet*. **2**, 271–280 (1976).

107. L.T. Boni, S. T. Hui, The mechanism of polyethylene glycol-induced fusion in model membranes. (1987).

108. T. Hossein, K. Kaylan, T. Bersano-Begey, K. E. Luker, G. D. Luker, S. Takayama, Rehydration of polymeric, aqueous, biphasic system facilitates high throughput cell exclusion patterning for cell migration studies. *Adv. Funct. Mater*. **21**, 2920–2926 (2011).

109. H. Tavana, B. Mosadegh, S. Takayama, Polymeric aqueous biphasic systems for non-contact cell printing on cells: engineering heterocellular embryonic stem cell niches. *Adv. Mater*. **22**, 2628–2631 (2010).

110. Y. Fang, J. P. Frampton, S. Raghavan, R. Sabahi-Kaviani, G. Luker, C. X. Deng, S. Takayama, Rapid generation of multiplexed cell cocultures using acoustic droplet ejection followed by aqueous two-phase exclusion patterning. *Tissue Eng. Part C. Methods*. **18**, 647–657 (2012).

111. A.G. Teixeira, R. Agarwal, K. R. Ko, J. Grant-Burt, B.M. Leung, J. P. Grampton, Emerging biotechnology applications of aqueous two-phase systems. *Adv. Healthc. Mater*. **7**, 1701036 (2017).

112. H. Tavana, S. Takayama, Aqueous biphasic microprinting approach to tissue engineering. *Biomicrofluidics*. **5**, 13404 (2011).

113. J. G. Rheinwatd, H. Green, Serial cultivation of strains of human epidermal keratinocytes: the formation of keratinizing colonies from single cells. *Cell*. **6**, 331–343 (2018).

114. K. Kobayashi, A. Rochat, Y. Barrandon, Segregation of keratinocyte colony-forming cells in the bulge of the rat vibrissa. *Proc. Natl. Acad. Sci. U. S. A*. **90**, 7391–7395 (1993).

115. H. Zarkoob, S. Bodduluri, S. V Ponnaluri, J. C. Selby, E. A. Sander, Substrate stiffness affects human keratinocyte colony formation. *Cell. Mol. Bioeng*. **8**, 32–50 (2015).

116. A. B. Singh, R. C. Harris, Autocrine, paracrine and juxtacrine signaling by EGFR ligands. *Cell. Signal*. **17**, 1183–1193 (2005).

117. S. Pastore, F. Mascia, V. Mariani, G. Girolomoni, The epidermal growth factor receptor system in skin repair and inflammation. *J. Invest. Dermatol*. **128**, 1365–1374 (2008).

118. G. Maheshwari, H. S. Wiley, D. A. Lauffenburger, Autocrine epidermal growth factor signaling stimulates directionally persistent mammary epithelial cell migration. *J. Cell Biol*. **155**, 1123–1128 (2001).

119. M. Piepkorn, M. R. Pittelkow, P. W. Cook, Autocrine regulation of keratinocytes: the emerging role of heparin-binding, epidermal growth factor-related growth factors. *J. Invest. Dermatol*. **111**, 715–721 (1998).

120. H. Hirata, M. Samsonov, M. Sokabe, Actomyosin contractility provokes contact inhibition in E-cadherin-ligated keratinocytes. *Sci. Rep*. **7**, 46326 (2017).

121. C. Dietrich, J. Scherwat, D. Faust, F. Oesch, Subcellular localization of β-catenin is regulated by cell density. *Biochem. Biophys. Res. Commun*. **292**, 195–199 (2002).

122. M. C. C. Morais, I. Stuhl, A. U. Sabino, W. W. Lautenschalger, A. S. Queiroga, T. C. Tortelli, R. Chammas, Y. Suhov, A.F. Ramos, Stochastic model of contact inhibition and the proliferation of melanoma in situ. *Sci. Rep*. **7**, 8026 (2017).

123. A. Stockinger, A. Eger, J. Wolf, H. Beug, R. Foisner, E-cadherin regulates cell growth by modulating proliferation-dependent β-catenin transcriptional activity. *J. Cell Biol.* **154**, 1185–1196 (2001).

124. M. Pruniéras, M. Régnier, D. Woodley, methods for cultivation of keratinocytes with an air-liquid interface. *J. Invest. Dermatol*. **81**, S28–S33 (1983).

125. J. P. H. Smits, H, Niehues, G. Rikken, I. M. J. J. Van Vlijmen-Willems, G. W. H. J. F. Van de Zande, P. Zeeuwen, J. Schalkwijk, E. H. Van den Bogaard, Immortalized N/TERT keratinocytes as an alternative cell source in 3D human epidermal models. *Sci. Rep*. **7**, 11838 (2017).

APPENDIX A: Cambridge University Press Copyright License

CAMBRIDGE UNIVERSITY PRESS LICENSE
TERMS AND CONDITIONS

Apr 07, 2018

This Agreement between Dalhousie University -- Rishima Agarwal ("You") and Cambridge University Press ("Cambridge University Press") consists of your license details and the terms and conditions provided by Cambridge University Press and Copyright Clearance Center.

License Number	4323750958056
License date	Apr 07, 2018
Licensed Content Publisher	Cambridge University Press
Licensed Content Publication	MRS Advances
Licensed Content Title	Biopatterning of Keratinocytes in Aqueous Two-Phase Systems as a Potential Tool for Skin Tissue Engineering
Licensed Content Author	Rishima Agarwal, Kristin Robin Ko, Paul F. Gratzer, John P. Frampton
Licensed Content Date	May 15, 2017
Licensed Content Volume	2
Licensed Content Issue	45
Start page	2443
End page	2449
Type of Use	Dissertation/Thesis
Requestor type	Author
Portion	Full article
Author of this Cambridge University Press article	Yes
Author / editor of the new work	Yes
Order reference number	
Territory for reuse	North America Only
Title of your thesis / dissertation	Investigating the Use of Precision Cellular Biopatterning for Generating Functional Skin Equivalents
Expected completion date	Apr 2018
Estimated size(pages)	120
Requestor Location	Dalhousie University 5981 University Avenue PO BOX 15000 Halifax, NS B3H4R2 Canada Attn: Dalhousie University
Publisher Tax ID	123258667RT0001
Billing Type	Invoice

Billing Address	Dalhousie University 5981 University Avenue PO BOX 15000 Halifax, NS B3H4R2 Canada Attn: Dalhousie University
Total	0.00 CAD

Terms and Conditions

TERMS & CONDITIONS

Cambridge University Press grants the Licensee permission on a non-exclusive non-transferable basis to reproduce, make available or otherwise use the Licensed content 'Content' in the named territory 'Territory' for the purpose listed 'the Use' on Page 1 of this Agreement subject to the following terms and conditions.

1. The License is limited to the permission granted and the Content detailed herein and does not extend to any other permission or content.
2. Cambridge gives no warranty or indemnity in respect of any third-party copyright material included in the Content, for which the Licensee should seek separate permission clearance.
3. The integrity of the Content must be ensured.
4. The License does extend to any edition published specifically for the use of handicapped or reading-impaired individuals.
5. The Licensee shall provide a prominent acknowledgement in the following format: author/s, title of article, name of journal, volume number, issue number, page references, , reproduced with permission.

Other terms and conditions:
v1.0

Questions? customercare@copyright.com or +1-855-239-3415 (toll free in the US) or +1-978-646-2777.